Carbon Trends 16 (2024) 100384

Contents lists available at ScienceDirect

Carbon Trends

journal homepage: www.elsevier.com/locate/cartre

Layered double hydroxides and metal-organic frameworks for electrocatalytic CO_2 reduction: A comprehensive review

Mahider Asmare Tekalgne [a,1], Ha Huu Do [b,1], Gyeong Ho Han [c,1], Sung Hyun Hong [a], Jin Hyuk Cho [a], Sang Hyun Ahn [c,*], Soo Young Kim [a,*]

[a] M Department of Materials Science and Engineering, Institute of Green Manufacturing Technology, Korea University, 145 Anam-ro, Seongbuk-gu, Seoul 02841, Republic of Korea
[b] VKTech Research Center, NTT Hi-Tech Institute, Nguyen Tat Thanh University, Ho Chi Minh City 700000, Vietnam
[c] School of Chemical Engineering and Materials Science, Chung-Ang University, 84 Heukseok-ro, Dongjak-gu, Seoul 06974, Republic of Korea

ARTICLE INFO

Keywords:
Layered double hydroxides
Metal-organic frameworks
Electrocatalysis
Co_2 reduction
Renewable energy

ABSTRACT

Electrocatalytic carbon dioxide (CO_2) reduction has emerged as a promising approach for converting CO_2 into value-added products and mitigating greenhouse gas emissions. Layered double hydroxides (LDHs) and metal-organic frameworks (MOFs) have attracted significant attention as potential electrocatalysts for CO_2 reduction due to their unique structural properties and tunable chemical compositions. In this review, we provide a comprehensive overview of recent advances in the utilization of LDHs and MOFs as electrocatalysts for CO_2 reduction. Scrutiny on various catalysts, along with their general design ways for CO_2 reduction is presented. This review will provide insight into the up-to-date research progress in MOF-based materials for CO_2 conversion. Furthermore, we highlight opportunities in this field and propose future research directions aimed at optimizing the performance of LDHs and MOFs for CO_2 reduction applications.

1. Introduction

The combustion of fossil fuels has indisputably contributed to the greenhouse effect by releasing a considerable amount of CO_2 into the atmosphere, leading to the serious climate change [1,2]. To address this issue, numerous strategies have been employed in attempts to treat CO_2 gas. Carbon capture and storage (CCS) technologies keep a vital function in preventing CO_2 from entering the atmosphere. This approach can eliminate approximately 90 % of the CO_2 created from the burning of the oil, coal, and natural gas, which provides energy for sustaining human life [3–5]. However, the high cost of CO_2 storage and transportation is still remained a significant challenge [5]. An alternative approach for dealing with this problem is to convert CO_2 to useful chemicals via electrochemical reduction methods. These approaches for CO_2 reduction involves a multiple reaction process necessitated by the thermodynamic stability of the CO_2 molecules. In a CO_2-saturated aqueous solution, these reactions are more challenging than the splitting of water, owing to their sluggish kinetics and energy-intensive reduction [6]. Furthermore, it is exceedingly difficult to decrease the anion radical (CO_2^-) to other useful chemicals. Therefore, catalysts that can accelerate reactions at a potential near the equilibrium and facilitate selective CO_2 conversion (rather than H^+) are essentially needed.

Electrocatalytic CO_2 reduction reaction (CO_2RR) can generate useful products such as CO, CH_3OH, CH_4, and C_2H_5OH [7–12], which can provide an efficient storage method for electricity generated from renewable energies, complementing their intermittence [13,14]. The first electrocatalytic CO_2 reduction was reported in 1870 using Zn electrodes to produce HCOOH, followed by several studies with other metals such as Sn, In, Pd, and Cd [15,16]. In 1994, Hori et al. have reported that the product selectivity was varied, significantly depending on the elements of pure metal catalysts [17]. For example, the CO can be selectively produced with Au, Ag, and Zn catalysts, whereas the Sn, In, and Pb catalysts are effective to produce formate ($HCOO^-$) [18]. Computational study based on density functional theory (DFT) revealed that the selectivity of final products are governed by binding energy of reaction intermediates such as *COOH or *OCHO [19,20]. In addition, it was revealed that the C—C coupling of reaction intermetidate is a key to produce C_{2+} products [21,22]. Thus, various strategies have been

* Corresponding authors.
E-mail addresses: shahn@cau.ac.kr (S.H. Ahn), sooyoungkim@korea.ac.kr (S.Y. Kim).
[1] M. Tekalgne, H. H. Do, and G. H. Han contributed equally to this work.

https://doi.org/10.1016/j.cartre.2024.100384
Received 18 March 2024; Received in revised form 10 May 2024; Accepted 12 June 2024
Available online 22 July 2024
2667-0569/© 2024 The Authors. Published by Elsevier Ltd. This is an open access article under the CC BY-NC-ND license (http://creativecommons.org/licenses/by-nc-nd/4.0/).

conducted to develop the high-performance catalyst with high activity and selectivity, which can be tuned by size, morphology, composition, oxidation state, grain boundary, and facet [23]. These catalysts are advantageous to control the electrochemical surface area (ECSA), intrinsic activity, and local pH, resulting the high selectivity for desired products at low overpotential.

Developing efficient catalysts for CO_2 conversion processes requires a combination of different materials, while ensuring high catalytic performance and durability for large-scale production [24]. Over the last decade, significant research has focused on exploring the unique properties of graphene, sparking interest in various 2D materials like transition metal dichalcogenides (TMDs) [25,26], MXenes [27], and oxides [28]. These materials have garnered attention for their diverse properties and potential applications across science and engineering. Recently, layered double hydrooxides(LDHs) and metal-organic frameworks (MOFs) are widely used in electrochemical energy storage and conversion.

Layered metal hydroxides encompass a diverse range of layered materials, including single-metal layered hydroxides and layered double hydroxides (LDHs) characterized by positively charged host layers resembling brucite, interspersed with exchangeable interlayer anions (Fig. 1). Their chemical formula can be represented as $[M^{2+}_{1-x}M^{3+}_{x}(OH)_2]^{x+}(A^{n-})_{x/n}\cdot mH_2O$. The host layers typically consist of divalent metal cation (e.g., Ni^{2+}, Mg^{2+}, Fe^{2+}, Co^{2+}, etc.) octahedrally coordinated with hydroxyl groups, with a fraction being replaced by trivalent metal cation (e.g., Mn^{3+}, Fe^{3+}, Al^{3+}, Cr^{3+}, etc.). The interlayer anion A^{n-} denotes an interlayer anions such as CO_3^{2-}, NO^{3-}, ClO^{4-}, acetate and etc. to balance the charge of the host layer. The interaction between the anion and the LDH layer, facilitated by electrostatic forces and hydrogen bonds, gives LDHs intriguing anionic exchange capabilities, making them highly versatile for various applications. For example, anion exchange in ZnAl-LDHs synthesized on a silicon substrate was evaluated using a posttreatment-based reconstruction method. The result indicated that the calcined ZnAl-LDH went reconstruction due to anion exachne with NaCl. Increasing NaCl concentration from 0.15 M to 0.60 M resulted in higher rates of anion exchange, but above 0.90 M, anion exchange decreased. This suggests that controlling NaCl concentration during the reconstruction process can modify the anion composition and shape of ZnAl-LDHs [29]. It's key to note that the flexibility in composing LDH layers is somewhat limited, primarily due to the size and charge constraints of the cations that can be incorporated into the layer structure.

The discovery of metal organic frameworks (MOFs) materials has introduced its potential in fascinating environmental applications and practical devices. MOFs are built from metal ions (e.g., Co^{2+}, Zn^{2+}, Ni^{2+}, Cu^{2+}, M^{2+}) and organic linkers (carboxylate, sulfonate, phosphonate) (Fig. 2) [30]. Therefore, by combining a wide variety of metal ions and organic linkers, an abundance of adaptable and responsive MOF materials is created. Currently, over 20,000 MOF structures are described in the literature [31,32] for various applications including gas adsorption [33–35], catalysis [36–38], sensors [39–41], and drug delivery [42] because of their special properties such as ultrahigh surface area and tunable architecture [43]. Particularly, the MOFs having transition metal sites are utilized as efficient catalysts in electrochemical energy

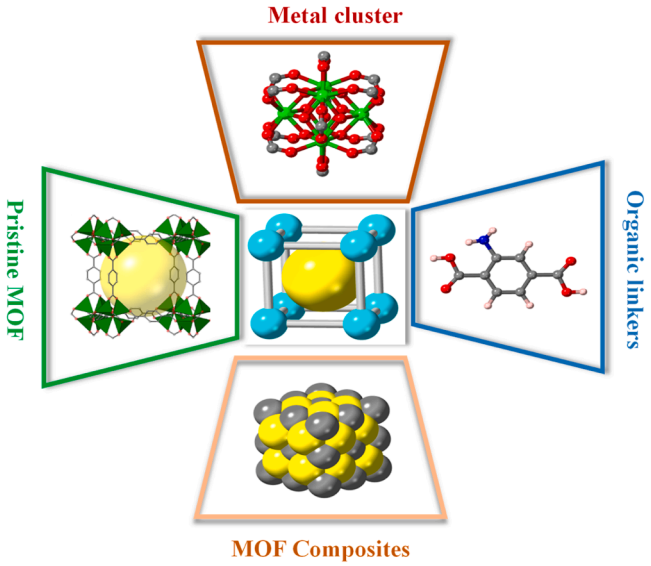


Fig. 2. Structure of pristine MOF, metal cluster, organic linkers and MOF-composites.

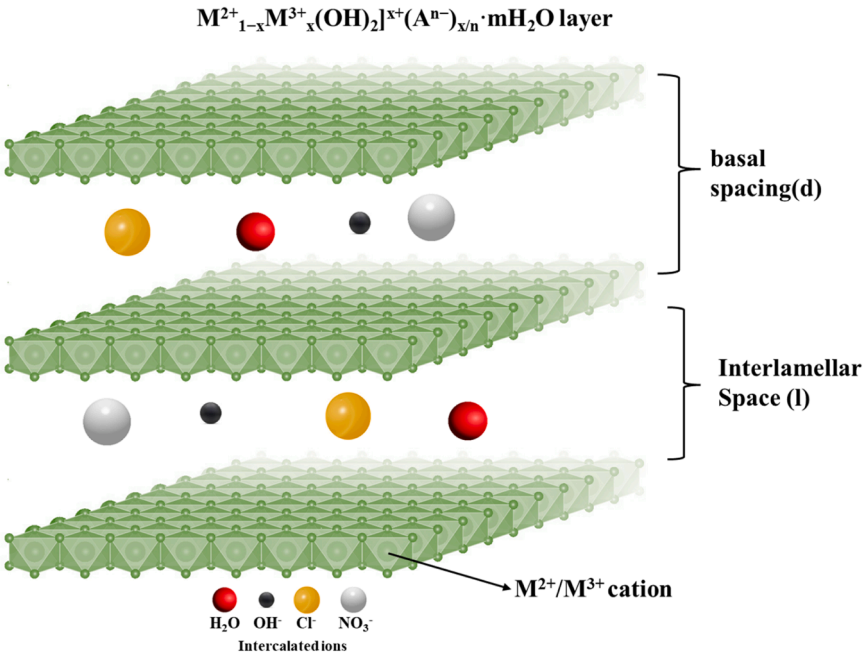


Fig. 1. Structure of layered double hydroxides (LDHs).

conversion, involving the hydrogen evolution reaction (HER) [44–46], oxygen reduction reaction (ORR) [47–50], and CO_2RR [51–62]. Furthermore, the catalytic activity of MOFs can be altered by adding functional groups to organic linkers. For instance, Fu et al. altered the property of MIL-125(Ti) by amino groups for converting CO_2 to formate [63]. The results revealed that NH_2–MIL-125(Ti) displayed an improved catalytic performance over MIL-125(Ti). In addition, Guo et al. [64] used metal nanoparticle stabilizer in amino functionalized UiO-68 MOF and which showed an excellent photocatalytic CO_2 reduction.

Herein, we present a comprehensive work of the recent literature on LDHs and MOF-related catalysts for electrocatalytic CO_2RR. This review article draws from the knowledge presented in previous great review publications on similar issues, with detailed discussion related to LDHs and MOF-based catalysts. It begins with a brief allusion in the basic theory and crucial criterion of CO_2RR by the electrochemical method and discusses on various LDHs and MOF-based catalysts for electrochemical CO_2RR and their design ways.

2. Fundamentals and challenges of CO_2RR

2.1. Electrocatalytic CO_2RR

2.1.1. Basic mechanism

Electrocatalytic CO_2RR has been recognized as a potential strategy to transform CO_2 to precious chemicals. This process includes multiple reactions at various potentials, as shown in the electrochemical reactions occurred in the electrocatalytic CO_2 reduction with water at pH 7 and their redox potentials are presented in Table 1. As a result, the obtained products are considerably diverse, involving methane, methyl alcohol, carbon monoxide, methyl aldehyde, formic acid, and ethylene, as shown in Fig. 3a. The electrochemical reduction of CO_2 can occur through pathways involving two, four, six, eight, or twelve electrons Fig. 3b. In this process, HER is inevitable during CO_2 reduction, which decreases the catalytic performance of CO_2 conversion [65]. Density functional theory (DFT) calculation was recognized as an efficient method for finding the mechanism of chemical reactions. In terms of electrochemical applications, DFT is usually used to determine the binding energies of intermediates and activation energy, which is useful to estimate the reaction pathway. For example, the free energy of hydrogen adsorption is calculated to predict the catalytic activity for HER [66]. In comparison, CO_2 conversion by the electrocatalytic method is more complicated than hydrogen production due to its various reduction adducts. Thermochemical models have been investigated for determining the CO_2 reduction reaction mechanism [67]. However, this task is a great challenge due to the complication of the electrochemical process. Therefore, the generation of desirable products is one of the most daunting challenges in electrocatalytic CO_2RR.

The mechanism of electrocatalytic CO_2RR includes three principal steps. The first step illustrates the adsorption of CO_2 onto the surface of the catalyst. The CO_2 receives electrons in the second step, which result in the breakage of C–O bonds, thus playing a vital role in the electrocatalytic CO_2RR. This process can be accompanied by proton migration to form a C—H bond. Finally, the products are obtained via desorption from the face of the catalyst. The proposed mechanisms for the formation of different products. The obtained product depends on various factors, such as applied voltage [68], electrolyte [69], and pressure [70]. For example, Thorson's study revealed that electrolytes containing large cations enhance the catalytic performance of transforming CO_2 to CO [71]. Ogura et al. scrutinized the influence of halide anions, including Cl^-, Br^-, and I^- on the yield of electrocatalytic CO_2RR on a copper electrode [72]. They found that these anions can be adsorbed onto the Cu electrode to create catalytic layers. These layers facilitate electron transfer for CO_2 reduction, leading to increased current density. In addition, this phenomenon prevents proton adsorption which would have otherwise led to the HER. Furthermore, the type of catalyst has a vital function in the generation of desirable chemicals. For instance, numerous studies have indicated that Ag, Au, Zn, Pd, and Ga are suitable for converting CO_2 to CO, while Cd, Hg, In, Pb, Sn, and Tl are favorable for HCOOH formation [73].

Table 1
The reduction potential of half reactions in electrocatalytic CO_2 reduction reaction (under condition of pH 7 in aqueous solution versus a standard hydrogen electrode (SHE), 25°C, 1 atm gas pressure, and 1 M for other solutes) [185,186].

No.	Half reactions of CO_2 reduction	Redox potential (V vs. SHE) at pH = 7
(1)	$CO_2 + e^- \rightarrow CO_2^{*-}$	−1.9
(2)	$CO_2 + 2H^+ + 2e^- \rightarrow HCOOH$	−0.61
(3)	$CO_2 + 2H^+ + 2e^- \rightarrow CO + H_2O$	−0.53
(4)	$CO_2 + 4H^+ + 4e^- \rightarrow HCHO + H_2O$	−0.51
(5)	$CO_2 + 6H^+ + 6e^- \rightarrow CH_3OH + H_2O$	−0.38
(6)	$CO_2 + 8H^+ + 8e^- \rightarrow CH_4 + 2H_2O$	−0.24
(7)	$2CO_2 + 12H^+ + 12e^- \rightarrow C_2H_4 + 4H_2O$	−0.34
(8)	$2H^+ + 2e^- \rightarrow H_2$	−0.42

2.1.2. Main parameters for evaluating catalytic activity in CO_2RR

This section describes the main parameters that are utilized to assess the quality of catalysts, including onset potential, Tafel slope, turnover frequency (TOF), Faradaic efficiency (FE), partical current density, and stability.

Onset potential: This quantity was recognized as an initial evaluation parameter for electrocatalytic performance. The onset potential is recorded at the point where the current of the reaction changes from the background signal [74].

Tafel slope: Tafel slope is the slope of the Tafel equation ($\eta = b^*\log i + a$, where η is overpotential, i is current density and b is Tafel slope), which provides the relation between the current density and the overpotential. It can be obtained from the graph using the Tafel equation. Moreover, a proposed reaction mechanism can be based on the Tafel slope [75]. A good electrocatalyst exhibits a small Tafel slope.

TOF: It determines the how fast an electrochemical reaction is happening per active electrocatalytic center at a specific overvoltage and allows for the exploration of intrinsic activity of electrocatalysts. It is very difficult to determine the TOF quantity of electrocatalysts, except for a few noble metals (e.g., Pt and Pd) where their surface-active site can be quantified, following their structural indistinctness of the active centers. Enormous efforts regularly undertaken that all used catalysts productively take part in the electrochemical process. Therefore, the derived TOF quantities are underrated, nevertheless they might suggest some understandings into the intrinsic activity.

FE: This quantity represents the efficiency of charge transfer in the electrochemical reaction. It is defined as the ratio of the experimental amount of generated product and the theoretical amount of generated product. An excellent catalyst typically exhibits an FE higher than 80 % towards the production of CO, CH_4, CH_3OH and other similar useful products [43,76].

2.1.3. Influence factors of CO_2 reduction performance

The factors that affect the catalytic CO_2 reduction performance can be divided into two aspects: properties of catalysts (crystal surface, interface effect, morphological structure, particle size) and reaction conditions (electrolyte, applied potential, temperature and pressure).

Crystal surface: enormous works have revealed that the selectivity of CO_2 reduction relies on the surface facet of the catalyst. It is found that Cu(110) facet facilitates for the formation of C_{2+} products with high faradaic efficiency, whereas Cu(100) is attributed to the enhance the performance of ethylene [77–79]. Another work revealed that the formation of CO on Ag(110) is better than that on Ag(111) facet [80].

Interface effect: interfacial interaction that was made from contact and synergy of various compositions of catalyst contribute to the alter binding energy and boosting electron transport. Thus, catalytic activities

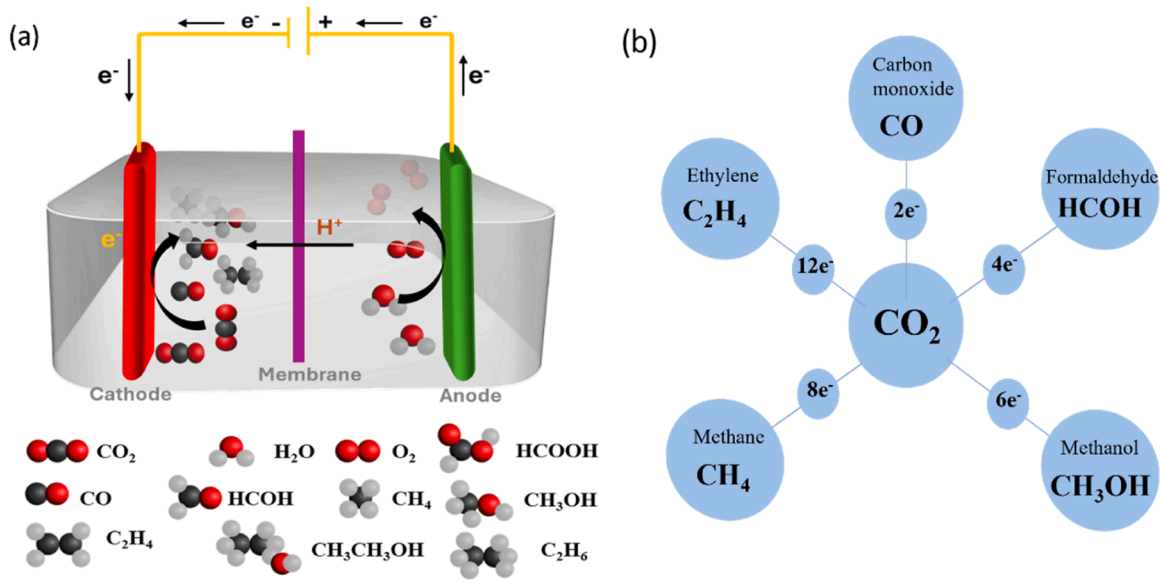


Fig. 3. (a) Graphical illustration and b) Electron processes involved in electrocatalytic CO_2 reduction reaction.

will vary in CO_2 reduction process. For example, Gao et al. Fabricated a metal/metal oxide hybrid structure that exhibited higher performance than that of metal and metal oxide for electrochemical CO_2 reduction. This was attributed to the interfacial effect of metal and metal oxide [81].

Structure effect: the change of morphological structure alters the roughness and specific surface area of catalysts, leading to the impact of the activity and selectivity of CO_2 reduction. Jiang and coworkers found that the O_2 plasma treatment alter the roughness of the Cu sheet, and improved the unsaturated Cu active centers. This result facilitates the formation of OCCOH*, leading to produce C_{2+} products [82]. Also, the effectiveness of hollow structures for CO_2 conversion is confirmed by many studies due to their large surface area and exposed abundant active centers [83–85].

Particle size: the change of size impacts to catalytic activities of the bulk phase catalyst. Because when the particle size reduces, under-coordinated surface sites and chemisorption increase exponentially, leading to performance variations. Reske found that accelerated when Cu nanoparticles are smaller than 5 nm the performance and selectivity of CO and H_2 were significantly [86].

Electrolyte: the selection of electrolyte for the CO_2 reduction process need to be considered because of it relates to the electrostatic forces and buffer capacity. A large number of studies used bicarbonate-based electrolytes ($KHCO_3$, $NaHCO_3$) for CO_2 reduction. Because they could create a bicarbonate-CO_2 complex, which plays a vital role in the accelerating CO_2 concentration on the surface of the catalyst. Besides, the characteristics of ions in solution influence performance and selectivity in CO_2 conversion. A trend was found that electrolytes having larger cations give a higher selectivity of C_{2+} products on Cu catalyst [87].

Applied potential: generally, the electrochemical reactions depend on the applied voltage. And CO_2 reduction process may occur many various reactions at different potentials. Thus, the influence of potential on efficiency needs to be evaluated to find optimal conditions with the highest FE for CO_2RR. Han et al. investigated the CO_2RR efficiency in a potential range of −1.9 – −1.45 V, indicating that the formation of CH_4 with the highest FE was recorded at −1.8 V [88].

Temperature and pressure: the change in temperature or pressure will affect the dissolution of CO_2 in the electrolyte, electrolyte resistance, and adsorption equilibrium. Therefore, numerous works were conducted to assess the factors. It is not easy to find a trend for an increase or decrease in temperature on the performance of CO_2RR., several articles revealed that the selectivity of CH_4 improves when the temperature reduces [89–94]. However, the trend of formation of the other products is not reported in detail. Besides, high-pressure influences the solubility of CO_2, causing the change in local CO concentration on the surface of catalysts, leading to the accelerated CO_2 reduction performance [95]. Despite reported several works on the impact of temperature pressure, systematic studies need to be conducted to further understand for CO_2RR.

3. Layered double hydroxide(LDH) based catalysts for electrocatalytic CO_2 reduction

3.1. Structure and properties of LDHs

Layered double hydroxides (LDHs) has a structure comprising positively charged host layers and matchable interlayer guest anions [96]. The host layers consist of edge-sharing metal hydroxide octahedra coordinated by divalent (M^{2+}) and trivalent (M^{3+}) metal cations, with the molar ratio of $M^{2+}/(M^{2+}+M^{3+})$ (denoted as X) being a critical factor for crystallization [96–98]. They exhibit fascinating properties due to the interaction between the positively charged layers and the interlayer anions, which facilitate anionic exchange reactions. This exchange ability, crucial for various applications, is governed by the affinity between the anion and the LDH host layer. Nitrate and chloride intercalated LDHs are particularly favored precursors for anion exchange reactions due to their specific affinity order. Factors such as time, temperature, and excess amount of anion influence the efficiency of the exchange reaction, making it a versatile method for modifying LDH properties.

The chemical and thermal stability of LDHs are crucial considerations for their practical applications, particularly those involving transfer, transport, and delivery. The chemical stability, often linked to the solubility of metal hydroxides, varies depending on the LDHs composition [99]. For instance, magnesium-based LDHs exhibit higher solubility compared to zinc-based ones due to differences in their solubility products [100]. Additionally, the interlayer anion influences the solubility of LDHs phases, as evidenced by thermochemical data. Regarding thermal stability, the decomposition behavior of LDHs follows specific trends depending on the metal ions involved, with different LDH compositions undergoing distinct mass loss events during thermal treatment [101]. Understanding the chemical and thermal stability of LDHs is crucial for optimizing their performance in various applications,

ranging from catalysis to materials science.

LDHs nanosheets possess a unique lamellar structure with easily regulated chemical composition and electronic structure, making them promising candidates for electrocatalysis. Density functional theoretical (DFT) calculations have revealed the electronic structures of various LDH nanosheets incorporating transition metals (TMs) such as CoFe, CoNi, NiFe, and ZnCo shedding light on their electrocatalytic behavior [102]. The research delved into the impact of electron-spin polarization on the electrocatalytic performance of these LDHs. Notably, a pronounced spin polarization effect was observed, facilitating electron transfer across the materials. Each of the TM LDHs exhibited a narrow bandgap, indicating their potential for electron mobility. However, ZnCo-LDHs stood out with a relatively larger bandgap, primarily attributed to the d atomic orbitals of Co, which hindered electron transfer. Consequently, the electron conductivity of ZnCo-LDH nanosheets was weakened, resulting in diminished electrocatalytic activity compared to the other LDH variants studied. Moreover, Surface modifications and defect engineering further allow for fine-tuning of the electronic structure, enhancing electron transfer efficiency and catalytic activity [103]. For example, oxygen vacancies, characterized by unoccupied bonding t_{2g} orbitals of the MO_6 center (MO_{6-x}), endow LDHs with heightened electronic conductivity and remarkable adsorption capacity for oxygen-related intermediates [104]. Conversely, metal vacancies, stemming from the varied electron and orbital distributions of metal atoms, result in an elevation of the valence state of neighboring metal centers, thereby influencing the catalytic behavior of the material.

The regulation of ions has emerged as a viable strategy for fine-tuning the electronic configuration, notably through anionic doping or replacement [105]. Huang et al. introduced sulfion, an anionic species with distinctive polarization characteristics, into CoAl–LDHs, thereby facilitating the adjustment of ion-covalent properties through the formation of Co-O bonds and Co-S dangling bonds (Fig. 4a) [106]. This sulfion-mediated regulation effectively modulates the electronic structure surrounding the active sites, enhancing their catalytic performance. Concurrently, Sun et al. demonstrated that the replacement of interlayer anions can exert a profound influence on the electronic configuration of exposed surface metal atoms in transition metal (TM) LDH nanosheets [107]. Specifically, anions with lower redox potentials, such as hypophosphites, facilitate the transport of electrons to the hydroxide layers, thereby increasing electron density and sustaining high-valence states of metal sites (Fig. 4b and c). This controlled electron transfer mechanism holds promise for optimizing the catalytic efficiency of LDH-based materials.

3.2. Synthesis methods for LDHs

In here we will go over some of the ways that LDHs can be synthesized, such co-precipitation, hydrothermal synthesis, urea hydrolysis, and sol-gel procedures. LDH synthesis methods like co-precipitation and urea hydrolysis are well-established and suitable for industrial-scale production.

The co-precipitation technique is a primary method for synthesizing LDHs where a super-saturated solution of metal salts is utilized to simultaneously precipitate $M(OH)_2$ and $M(OH)_3$. In here, maintaining a basic pH (9–10) is crucial for effective hydrotalcite formation, as low pH may hinder metal precipitation while excessively high pH could cause metal dissolution. Subsequent thermal treatment and aging enhance crystallinity, forming a brucite-like positive sheet composed of divalent and trivalent cations with solvated interlayer anions. For instance, Jiang et al. successfully synthesized MgAl-LDH using a supersaturated co-preciptation method, yielding a mesoporous structure [108]. The rich surface active groups and large interlayer distances provided ample

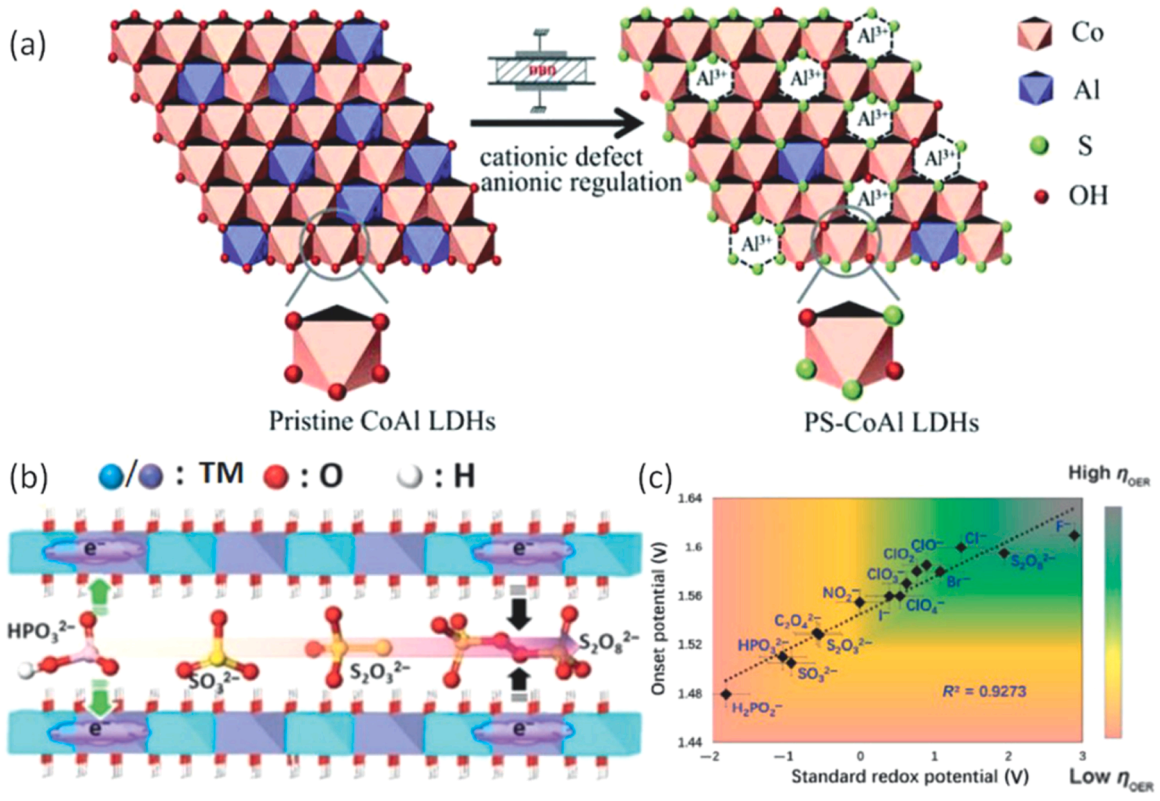


Fig. 4. (a) Illustration of the rapid preparation of CoAl LDHs with Al^{3+} vacancies and S^{2-} regulation by the modified water DBD plasma treatment. Reproduced with modifications with the permission of The Royal Society of Chemistry from Ref. [126]; (b) Electronic transfer between anion interlayer and hydroxide layers, (c) Relationship between onset potential and the standard redox potential of some common anions. Reproduced with modifications with the permission of Springer from Ref. [127].

active sites for NO_3 adsorption achieved ultrathin 2D nanosheets of CoFe-LDH catalysts through co-precipitation using hexamethylenetetramine as a precipitating agent, while Hussein et al. developed Mg/Al/Fe mixed oxides derived from layered-double-hydroxide (LDH) precursors using co-preciptation method which resulted in good redox activity for thermochemical CO_2 splitting with high CO prodiction rate [109]. Though, challenges arise with transition metals like Fe^{3+}, which tend to form gel-like hydroxides at low pH values complicating homogeneous precipitation, the use of urea or hexamethylenetetramine as hydrolysis agents, highly crystallized transition metal-LDHs microplates have been synthesized via hydrothermal methods.

The hydrothermal method, known for its simplicity, involves mixing metal salts and precipitating agents such as NaOH, Na_2CO_3, Urea, etc. in a Teflon container with solvents like water or organic solvents(such as ethanol, dimethyl formamide), followed by thermal treatment [110, 111]. It is noteworthy, the morphology, structure, and size of LDHs nanocrystals can be affected by concentration of hydroxyl anions, reaction temperature, and time respectively. This method, although versatile, lacks precise control over LDH growth and composition due to sealed reaction conditions. Wang et al. produced $Ca_2Al\text{-}NO_3$ and $Mg_3Al\text{-}CO_3$ LDHs using a continuous-flow hydrothermal methodwhere the particle size and shape were controlled by the recation temepratute and pressure [112]. The hydrothermal process can be modified by using urea as a precipitating agent in urea hydrolysis, which can be regulated to produce ammonium cyanate (NH^{4+}) and NCO^- in aqueous solutions [113].

Another notable approach involves electrochemical deposition, as demomnstrated by jin et al. enabling the synthesis of Ni-Co LDHs with a coaxial nanotube array structure [114]. Typically, this method involves the formation of self-supported LDH films on conductive substrates using two or three-electrode setups. Conductive substrates serve as cathodic sites for electro-precipitation, while a metal aqueous solution, often containing nitrate or sulfate ions, serves as the electrolyte. Applying a negative potential triggers cathodic currents via water reduction, leading to the precipitation of LDHs. Furthermore, factors such as metal salt types, temperature, deposition current, and salt concentration significantly influence the phase composition, morphology, and crystallinity of hydroxides or LDHs. This technique emerges as a straightforward, time-saving, and eco-friendly approach to LDH synthesis. Additionally, recent advancements in microwave-assisted methods have also broadened the horizon of LDH synthesis, introducing diverse structures such as core-shell, nanocone, and nanoflower configurations. Microwave treatment enables quick processing, leading to improved crystallinity and high specific surface areas [115]. The mechanism involves smaller particles dissolving and precipitating onto larger existing crystals, resulting in more abundant and well-crystallized materials. Microwave heating ensures uniform heating due to the interaction of microwaves with materials, promoting dipole re-orientation in dielectrics and reducing thermal gradients typically seen in conventional heating methods [116]. Moreover, the exfoliation of bulk LDHs presents a top-down approach to obtain LDHs nanosheets, with liquid exfoliation methods leveraging ultrasonic assistance for delamination [117]. Plasma technology also emerges as a promising method for LDHs nanosheet preparation, harnessing high-energy active particles to break interlayer connections and obtain ultrathin LDHs nanosheets [118].

3.3. Electrocatalytic performance of LDHs for CO_2 reduction

In this segment, we discuss some key examples of LDH-based electrocatalysts emphasizing their robust performance in CO_2 reduction as their structure shows great. Morphology, composition, and structure are pivotal in defining LDH functionality, with tailored properties enabling superior electrocatalyst design. Modification of LDHs interfaces enhances heterostructure activity, while chemically-exfoliated LDH nanosheets offer uniform shape and size, crucial for catalytic efficacy. LDH's brucite section allows versatile tuning of metal components, heteroatom doping, and defect engineering, optimizing electron transport and active site activity. Various fabrication strategies cater to LDHs unique 2D platform, enabling versatile nanoscale heterostructure manufacturing.

3.3.1. LDH for CO_2 conversion into methane and methanol

Nickel, known for its cost-effectiveness and availability, is a key component in catalysts used for the methanation process [119]. Traditional methods like incipient wetness impregnation (IWI) are commonly employed for catalyst preparation. However, catalysts synthesized through the IWI method often exhibit larger nanoparticle sizes and poor metal dispersion, leading to poor reaction rates and limited catalytic stability over time. To address these drawbacks, researchers have turned to layered double hydroxides (LDHs) as promising precursors for catalyst synthesis. LDHs offer a unique atomic-scale arrangement of cations and anions, making them ideal candidates for preparing catalysts with highly dispersed nanoparticles, even at high metal loadings. The formation of highly dispersed metal nanoparticles within the LDH-derived mixed oxide matrix enhances catalytic stability by promoting efficient metal-support interactions [120]. This strong interaction helps mitigate issues such as nanoparticle aggregation and metal leaching, which are common concerns in catalysts prepared using conventional methods. Consequently, catalysts derived from LDH precursors exhibit improved performance and longevity in methanation reactions, making them highly desirable for industrial applications requiring stable and efficient catalytic processes. For example, Guo et al. syntheiszed highly dispersed Ni catalysts supported on metal oxides with different Ni^{2+}/Al^{3+} molar ratios for CO_2 methanation (Fig. 5a) [121]. The as prepared cataltyst had the highest catalytic activity, converting 89.4 % CO_2 and selecting 99 % CH_4 at low temeprtaure (Fig. 5c and d). Its enhanced catalytic activity at low temperatures was attributed to its basic property, readily reducible NiO species, and synergistic effect between metal nanoparticles and base sites, rather than surface area. Adjusting the Ni^{2+}/Al^{3+} ratios facilitated control over the reducing property and base site density. In another study, NiAl-LDHs were synthesized using NaY-zeolite as the source of aluminum, followed by the preparation of Ni-based catalysts embedded on an AlO_x substrate through an in-situ reduction of LDHs [122]. The AlO_x substrate provided effective isolation, enhancing the high-temperature stability of the Ni-based catalyst. The catalyst exhibited high performance, achieving CO_2 conversion and CH_4 selectivity of 87.5 % and 100 %, respectively. Importantly, the catalyst maintained its activity over 200 h of continuous reaction at 350 °C, attributed to the confinement provided by the AlO_x substrate, which mitigated undesired agglomeration and sintering of Ni particles. Further investigations involving Ni, Co, and Al-based catalysts prepared by coprecipitation revealed that the Ni-based catalyst outperformed the others, exhibiting CO_2 conversions of up to 90 % and complete CH_4 selectivity between 300 and 350 °C [123]. This superior performance of NiAl catalyst was mainly attributed to its higher density of basic sites, along with a larger surface area, smaller crystallite size, and enhanced reducibility. Conversely, the CoAl catalyst displayed a lower number of total basic sites, resulting in reduced interaction with CO_2 and consequently lower CO_2 conversion compared to NiAl, achieving 100 % CH_4 selectivity. Moreover, both catalysts demonstrated remarkable stability during a 300-minute time-on-stream at 400 °C, with no significant signs of deactivation observed. Moreover, both catalysts demonstrated remarkable stability for 5hr at 400 °C, with no significant signs of deactivation observed.

The conversion of CO_2 into methanol represents a promising method for sustainable fuel and chemical production and researchers have been concentrating their efforts on Cu, Zn and Al_2O_3 catalysts for decades due to the high activity of these catalysts as well as their cost-effectiveness. For example, hierarchical Cu/Zn/Al nanocatalysts to enhance methanol yield from CO_2 hydrogenation, leveraging LDHs nanosheets and metal-organic frameworks (MOF) nanoparticles as dual solid precursors were

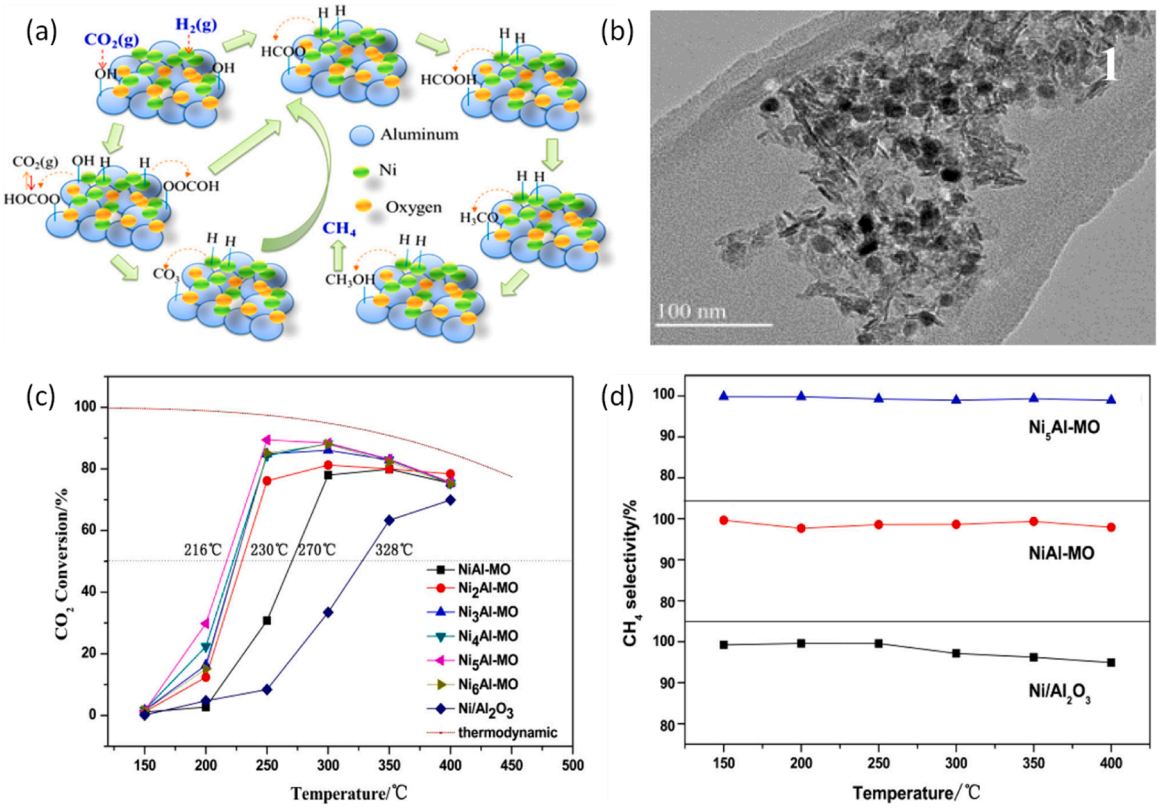


Fig. 5. (a) Schematic representation of CO_2 methanation by the NixAl-MO catalysts; (b) TEM images of NiAl-MO; (c) CO_2 conversion and (b) CH_4 selectivity for CO_2 methanation at different reaction temperatures over the as-prepared Ni_xAl-MO and Ni/Al_2O_3 catalysts. Reproduced with modifications with the permission of ACS publications from Ref. [129].

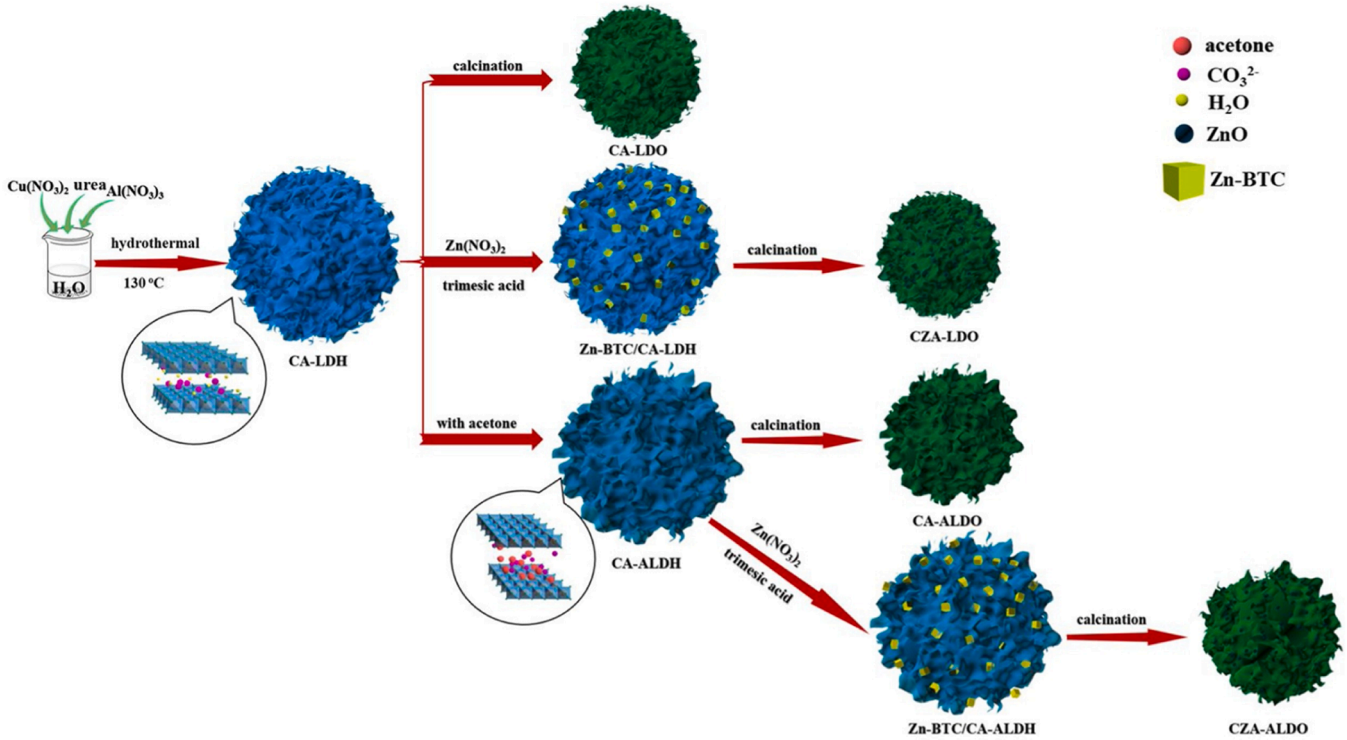


Fig. 6. Schematic representations of the steps used to make synthesis method used to prepare LDH, LDH/MOF. Reproduced with modifications with the permission of Elsevier from Ref. [132].

devised [124]. Through an in-situ growth approach under mild conditions, uniform deposition of Zn-BTC nanoparticles onto the surface of CuAl LDH can be achieved (Fig. 6). Interestingly, pretreating the LDH with acetone proved effective in exfoliating the sheet-like structure, augmenting specific surface area, and aiding in the immobilization of Zn-BTC nanoparticles. This optimization led to a significant enhancement in CO_2 hydrogenation performance, with methanol selectivity exceeding 90 %. In-situ DRIFTS analysis revealed that the promotion of methanol formation by ZnO, derived from Zn-BTC, primarily stemmed from the increased formation of $*CH_3O$ intermediates rather than *CO and *HCOO species on the catalyst surface. This comprehensive approach offers promising insights into improving the efficiency of CO_2 hydrogenation for methanol synthesis.

Recently, efforts have been made to integrate zirconium (Zr) into the conventional Cu-Zn catalyst system due to its ability to facilitate the formation of smaller copper particles, enhance copper dispersion, and help in the stabilization of active copper by inhibiting sintering and agglomeration during reaction [125]. In order to improve the catalytic performance of CuO-ZnO-ZrO_2, considerable attention has been directed towards dispersing it onto porous substrates like silica, alumina, and carbon nanotubes [126]. Among these, layered double hydroxides (LDHs) have emerged as a particularly promising support material due to their unique structure and properties. LDHs comprise metal hydroxide layers with a positive charge and interlayers with a negative charge, offering significant potential as catalyst carriers. In their studies, Fang et al. investigated a novel appraoch tilizing a layered double hydroxide (LDH), specifically Mg-Al LDH, as a carrier for Cu-ZnO-ZrO_2 catalysts via co-precipitation (Fig. 7a) [127]. Characterization revealed the formation of CuO-ZnO-ZrO2 nanoparticles uniformly dispersed and anchored onto the LDH surface (Fig. 7b). Notably, the catalyst exhibited a remarkable enhancement in both BET surface area and copper dispersion, leading to a dramatic methanol selectivity of 78.3 % (Fig. 7d). Remarkably, the CuO-ZnO-ZrO2 catalyst exhibited doubled space time yield based on active metal compared to commercial counterparts under mild reaction conditions, indicating heightened copper utilization efficiency facilitated by LDH. The observed performance enhancement may be attributed to the LDH-derived amorphous oxide's increased CO_2 adsorption capacity, enriching the concentration of adsorbed CO_2 near active metal sites.

3.3.2. *LDH for CO_2 conversion into carbon monoxide(CO)*

Theoretical studies highlight the involvement of diverse intermediates in CO production on catalyst surfaces during CO_2 electrocatalytic reduction, combining electrochemical and thermochemical reactions (Eqs. (1-3)) [128]. Concurrently, hydrogen evolution reactions (HER) occur at the cathode, further influencing CO_2 reduction (Eqs. (4-5)).

$$CO_2+(H^++e^-)\rightarrow *COOH \quad (1)$$

$$*COOH+(H^++e^-)\rightarrow *CO+H_2O \quad (2)$$

$$*CO+H_2O\rightarrow CO(g)+H_2O \quad (3)$$

$$H^++e^-\rightarrow *H \quad (4)$$

$$*H+(H^++e^-)\rightarrow H_2 \quad (5)$$

Although Au/Ag based catalysts demonstrate high efficiency in CO_2 conversion to CO, their commercial viability is hindered by cost and stability concerns [129]. Layered double hydroxides (LDHs) offer unique advantages including interlayer anion exchangeability and tunability, yet suffer from drawbacks such as low electrical conductivity and stability. To address these limitations, graphene and its derivatives emerge as promising solutions due to their exceptional properties including ultra-thin structure, mechanical robustness, large surface area, and high electron transfer capacity. Incorporating LDHs onto conductive substrates enhances LDH conductivity, stability, and dispersion, ultimately offering a pathway to overcome the challenges associated with LDH-based electrocatalysis [130]. Liu's group synthesized nickel-doped layered boehmite (Ni-AlO(OH)$_3$) directly on reduced graphene oxide (RGO), forming composites with enhanced electrical conductivity and numerous active sites and promoting the formation of pore channels conducive to active site exposure, reactant/product adsorption, and desorption [131]. Ni-AlO(OH)$_3$@RGO exhibited the highest CO FE of 92.20 %, while AlO(OH)@RGO and Ni(OH)$_2$@RGO exhibited CO FE values of 44.9 % and 88.2 %, respectively, indicative of the significant enhancement in the efficiency of CO_2 reduction to CO facilitated by the combination of double metal hydroxide and nitrogen-doped RGO. The catalyst's outstanding performance stemmed from its abundant edge sites and defects, promoting the chemical adsorption of reactants and intermediates, while its high dispersion and extensive pore networks facilitated CO_2 and electrolyte transmission,

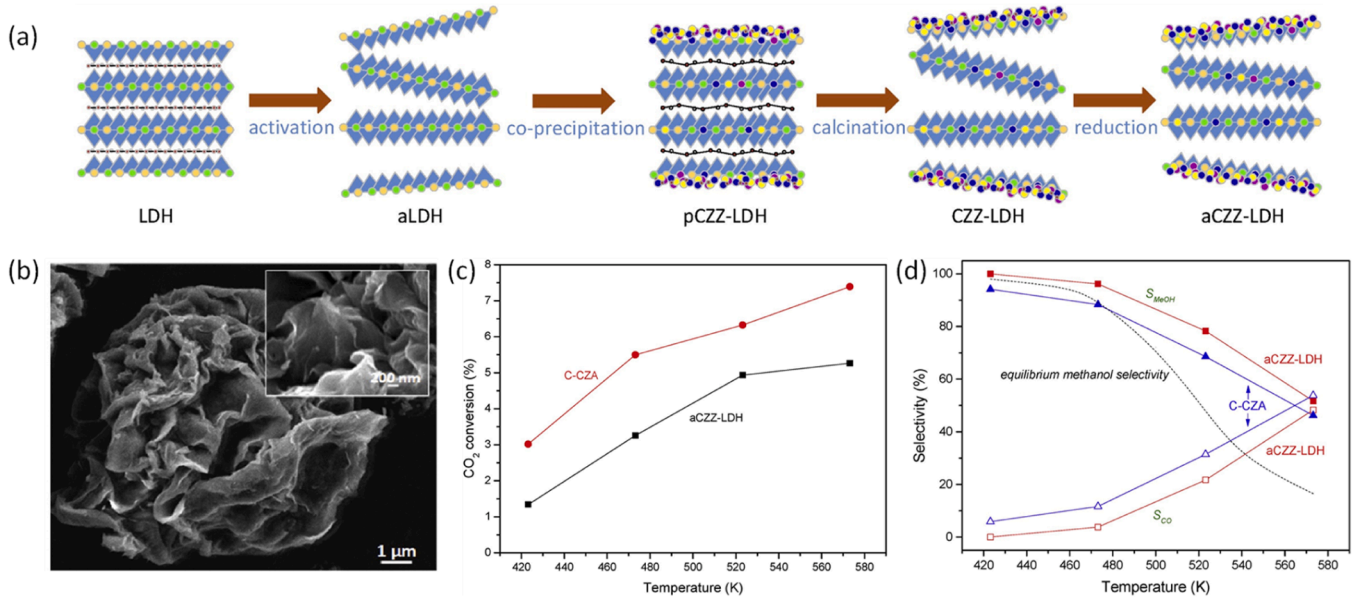


Fig. 7. (a) Schematic of CuO-ZnO-ZrO2 synthetic processes; (b) SEM images of CuO-ZnO-ZrO2 –LDH; (c) CO2 conversion and (d) Selectivity of methanol and carbon monoxide at various reaction temperatures. Reproduced with modifications with the permission of Elsevier from Ref. [135].

enhancing ECR reaction kinetics. In another study, CuMgAl-LDHs (Layered double hydroxides) served as precursors to produce supported Cu catalysts with excellent dispersion and stability (Fig. 8a). Reduction of CuMgAl-LDH at 400 °C resulted in the formation of CuMgAl-LDH, featuring well-dispersed Cu nanoparticles on MgO/Al_2O_3 [132]. Achieving a CO_2 conversion of 33.5 % with nearly 100 % selectivity to CO at 350 °C under high space velocity sets a new benchmark for Cu-based catalysts, particularly at lower reaction temperatures. In-situ DRIFTS and CO_2-TPD analyses (Fig. 8c) elucidated that its superior performance stems from the high Cu dispersion, facilitating H_2 dissociation, and the presence of diverse basic sites facilitating CO_2 adsorption for formate formation. This underscores the potential of LDHs in crafting supported metal catalysts. This comprehensive investigation underscores the versatility and efficacy of LDHs as precursor materials for developing advanced supported metal catalysts, showcasing their potential in green energy conversion processes. Furthermore, cadmium-aluminum layered bimetallic hydroxide nanoparticles (CdAl-LDHs) were synthesized via electrochemical deposition, offering insights into their electrocatalytic behavior [133]. Notably, CdAl-LDHs exhibited remarkable selectivity towards CO production in the presence of 2 %-BMIM(PF_6)/DMF electrolyte, showcasing a CO Faraday efficiency of 99.71 % and a CO partial current density of 22.13 mA cm^{-2}, rivaling or surpassing noble metal catalysts. In addition, the catalyst demonstrated exceptional stability over 30 h of continuous operation with minimal degradation throughout the reaction cycle. The synthesis method not only overcomes the limitations of traditional hydrothermal synthesis but also offers practical implications for industrial-scale electrocatalytic applications, underscoring the potential of CdAl-LDHs as cost-effective alternatives to noble metal catalysts.

4. Metal organic framework-based catalysts for electrocatalytic CO_2 reduction

During the last decades, research groups have extensively investigated the application of MOFs as catalysts for hydrogen production by electrochemical and photocatalytic pathway.

Scientists have scrutinized on the many unique features of MOFs, involving sizeable specific surface area, tunable architecture, rich morphological structure, easy modifying of the structural component, and act as the ideal platforms for the fabrication of different materials. Additionally, MOFs have been scrutinized as catalysts for hydrogen and oxygen production, and the electrochemical reactions were implemented in acidic and alkaline media. Summary of some MOF-based electrocatalysts for CO_2 reduction were provided in Table 2.

4.1. Structure and properties of MOFs

The different structure of MOFs such as 2D and 3D nanosheet provides large surface areas, high permanent porosity, exposed metal sites and guarantee accessible active centers for the adsorption CO_2 molecules which in return improves the electrocatalytic activity. In fact, MOFs have recorded the highest specific surface area and CO_2 storage of all porous material families [134–136,55]. In 2010, MOF-210 was successfully synthesized by Furukawa et al. [134]. This structure exhibited an ultrahigh pore volume of 3.6 $m^3\ g^{-1}$ and an excellent CO_2 uptake capacity of 2870 mg g^{-1}, that is the best among all reported studies. These features help CO_2 molecules access active sites on MOFs, thus facilitating improvement of catalytic activity for CO_2 reduction. In addition, the wide variety of chemical options encourages the tailoring of structural MOFs for specific applications [137,138]. Pristine MOFs can display catalytic activity on both metal nodes and organic components [139]. On the other hand, conductivity is important in electrocatalysis. Because electrical conductivity is a characteristic of a material that quantifies the effectiveness of the charge transport. Therefore, conductive MOFs have been developed for CO_2 reduction applications due to their high charge-carrier mobilities and adjustable catalytic/redox-active centers [140,141]. Moreover, MOFs having low conductivity usually are mixed with high conductive material (carbon black, graphene oxide) for enhanced electron transfer, leading to the accelerating electrochemical performance [142]. Beside, MOFs are ideal precursors to the well-distribution of metal nanoparticles in organic frameworks under operation condition, which accelerating for CO_2 reduction [143,144]. Furthermore, strategies such as size engineering [145], heterostructure formation [146–150] and new ligand structures

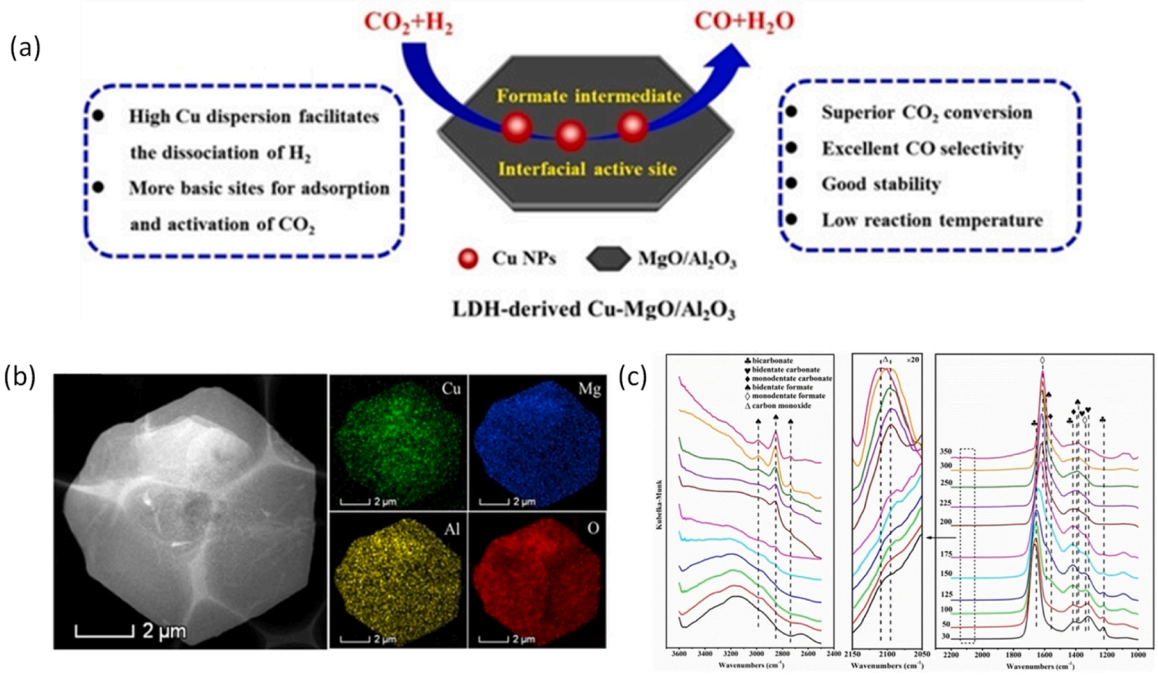


Fig. 8. (a) LDH- derived Cu-MgO/Al_2O_3; (b) HRTEM and Mapping images of CuMgAl-LDH-400; (c) In-situ DRIFTS of CO_2 hydrogenation over CuMgAl-LDH-400. Reproduced with modifications with the permission of Wiley from Ref. [151].

Table 2
Summary of MOF-based electrocatalysts for CO_2 reduction reaction.

Materials	Electrolyte	Product	FE [%]	Peak potential [V]	Current density (mA cm^{-2})	Ref.
Ni(Im) nanosheets 5 nm	0.5 M $KHCO_3$ (pH 7.2)	CO	78.8	−0.85 vs. RHE	7.0	[164]
TCPP(Co)/ZrBTB-PSABA	0.5 M $KHCO_3$ (pH 7.3)	CO	85.1	−0.769 vs. RHE	5.8	[165]
ZIF-8	0.5 M NaCl	CO	65	−1.14 vs. RHE	~ 5.3	[166]
ZIF-8	0.25 M K_2SO_4 (pH 4.2)	CO	81	−1.1 vs. RHE	~ 12.0	[167]
ZIF-108	0.25 M K_2SO_4 (pH 4.2)	CO	52	−1.3 vs. RHE	12.8	[167]
PCN-222(Fe)	0.5 M $KHCO_3$ (pH 7.3)	CO	91	−0.6 vs. RHE	1.2	[170]
$Al_2(OH)_2$TCPP-Co-MOF	0.5 M K_2CO_3	CO	76	−0.7 vs. RHE	~ 1.0	[168]
Co-PMOF	0.5 M $KHCO_3$ (pH 7.2)	CO	99	−0.8 vs. RHE	18.08	[187]
NNU-15	0.5 M $KHCO_3$ (pH 7.2)	CO	99.2	−0.6 vs. RHE	32.2	[169]
Cu-BTC	0.5 M $KHCO_3$	C_2H_5OH	10.3	−0.28 vs. RHE	10.0	[178]
Cu-BTC	0.01 M TBATFB/DMF	Oxalic acid	51	−2.5 vs. Ag/Ag^+	19.22	[176]
Cu_2(CuTCPP) nanosheet	1 M H_2O/0.5 M EMIMBF4	$HCOO^-$	68.4	−1.55 vs. Ag/Ag^+	3.5	[188]
CR-MOF	0.5 M $KHCO_3$ (pH 7.7)	HCOOH	> 98	−1.2 vs. SHE	21.5	[175]
0D Cu/C-1000	0.1 M $KHCO_3$ (pH 6.8)	CH_3OH	43.2	−0.3 vs. RHE	1.0	[184]
Cu_2O@Cu-MOF	0.1 M $KHCO_3$ (pH 6.8)	CH_4	63.2	−1.71 vs. RHE	8.4	[189]
ZIF-CNT-FA-p	0.1 M $NaHCO_3$	CO	100	−0.86 vs. RHE	7.7	[190]
Ag_2O/layered ZIF	0.25 M K_2SO_4	CO	80.6	−1.2 vs. RHE	32.5	[191]
Co/Zn ZIF derived Co-N_2	0.5 M $KHCO_3$ (pH 7.2)	CO	94	−0.68 vs. RHE	18.1	[192]
ZIF-8-derived NC	0.5 M $KHCO_3$	CO	95.4	−0.5 vs. RHE	5.5	[193]

[151,152] were also investigated to boost the electrocatalytic performances of MOF catalysts. The topic will be discussed with examples in the later part.

4.2. Synthesis methods for MOFs

Various synthesis methods for metal-organic frameworks (MOFs) are discussed, including solvothermal/hydrothermal [153,154], microwave [155], electrochemical [156], mechanochemical [157], and sono-chemical approaches. Their synthesis involves several factors such as reaction conditions, solvent choice, metal ions, organic ligands, and crystallization kinetics [158]. In addition, purification and activation steps are crucial, with purification necessary for catalytic applications to remove impurities [159]. Activation involves emptying pores, often challenging without damaging the framework. Factors such as initial component ratio and synthesis temperature can also influence properties like thermal stability.

The solvothermal/hydrothermal technique relies on the self-assembly of products from soluble precursors, originally applied in zeolite synthesis but now applied to MOFs such as ZIFs and MILs as well. The reaction takes place in sealed containers utilizing polar solvents and occurs at temperatures ranging from 50 to 260 °C, often lasting for hours or days. Teflon-lined autoclaves are employed for reactions needing temperatures above 400 °C. Higher temperatures aid bond formation and crystallization, influencing crystal shape, though prolonged reaction times can lead to product decomposition [160]. For example, Mokaya et al. synthesized organoclay and copper-based MOF via solvothermal method, with the organoclay obtained by intercalating thionin into Cameroonian clay [161]. The resulting Sa-TN_{50}/$Cu_3(BTC)_2$ composite demonstrated enhanced electrocatalytic behavior.

The microwave-assisted method relies on electromagnetic waves interacting with materials, enhancing energy efficiency to produce small metal and oxide particles. Solutions are heated by microwaves for an hour or longer to form nanosized metal crystals, although this method has not been widely used for crystalline MOF synthesis [162]. Nevertheless, it offers rapid synthesis and precise control over particle shape and size.

The mechano-chemical approach involves grinding chemicals to create coordination bonds at room temperature, often without solvents, resulting in 1D, 2D. The method accelerates reactions through mechanical forces, enhancing mass transfer, reducing particle size, and inducing localized heating showing promise as an alternative to traditional solvothermal synthesis, producing MOFs with high purity and porosity [163].

4.3. MOF for CO_2 conversion into carbon monoxide

4.3.1. 2D mof nanosheets

2D MOFs have emerged as a young member of the 2D material group. Compared to bulk MOFs, 2D MOF nanosheets have numerous outstanding properties, such as the capability to form ultrathin films, large surface areas, and accessible active centers, which enhance their performance in the area of catalysis. For instance, Wu et al. prepared 2D Ni (II) imidazole (Im)-based zeolitic imidazole framework (ZIF) nanolayers as electrocatalysts for CO_2RR [164]. 2D $Ni(Im)_2$ sheets with various thicknesses were synthesized using different centrifugation forces. The result indicates that the 2D $Ni(Im)_2$ having a thickness of five nanometer exhibits a high CO selectivity (FE_{CO} = 78.8 % at −0.85 V vs. RHE), whiles bulk $Ni(Im)_2$ exhibits an FE_{CO} of 33.7 %. The improved performance is ascribed to the increased surface-active site density from the bulk phase to the nanoscale. This work also examines the impact of ammonium hydroxide (NH_4OH) on the catalytic activity of the 5-nm-thick 2D $Ni(Im)_2$. The authors found that 5 ml of NH_4OH is an optimal volume for the synthesis of 2D $Ni(Im)_2$ at 5 nm and results in the best performance for CO_2RR.

Another 2D MOF was illustrated by Zhang et al. [165]. The authors grafted TCPP(Co) ((5, 10, 15, 20)-tetrakis (4-carboxyphenyl) porphyrin)) on a substrate of ZrBTB nanosheet, as shown in Fig. 9a. This catalyst exhibits a great TOF value of 4768 h^{-1} (at 0.919 V vs. RHE) and an FE_{CO} of above 77% (at 0.769 V vs. RHE), as displayed in Fig. 9b. In comparison, TCPP(Co) exhibits a relatively high FE_{CO} of 75.4 % (at −0.896 V vs. RHE). However, its overpotential is higher than that of TCPP(Co)/ZrBTB, implying a lower energy conversion, while CO is not found for ZrBTB. To enhance the catalytic activity of TCPP(Co)/ZrBTB nanosheets, various chemicals including p-(aminomethyl)benzoic acid (PABA), psulfobebzoic acid potassium (PSBA), and p-sulfamidobenzoic acid (PSABA) were grafted on the original material. The results reveal that TCPP(Co)/ZrBTB-PSABA produces the highest yield with FE_{CO} of 85.1 %, whereas the yields of TCPP(Co)/ZrBTB-PABA and TCPP (Co)/ZrBTB-PSBA are 78.7 % and 81.5 %, respectively. In addition, TCPP(Co)/ZrBTB-PSABA exhibits a TOF of 5315 h^{-1}, which is larger than that reported in the previous studies on MOF materials. The improved performance is attributed to the steric effect induced by the modifier molecules. These molecules cover Zr sites, impeding hydrogen production, thus facilitating CO_2 reduction.

4.3.2. 3DMOFs

4.3.2.1. Zinc-based MOFs. MOFs have been of interest in many areas due to their unique characteristics such as ultrahigh porosity and

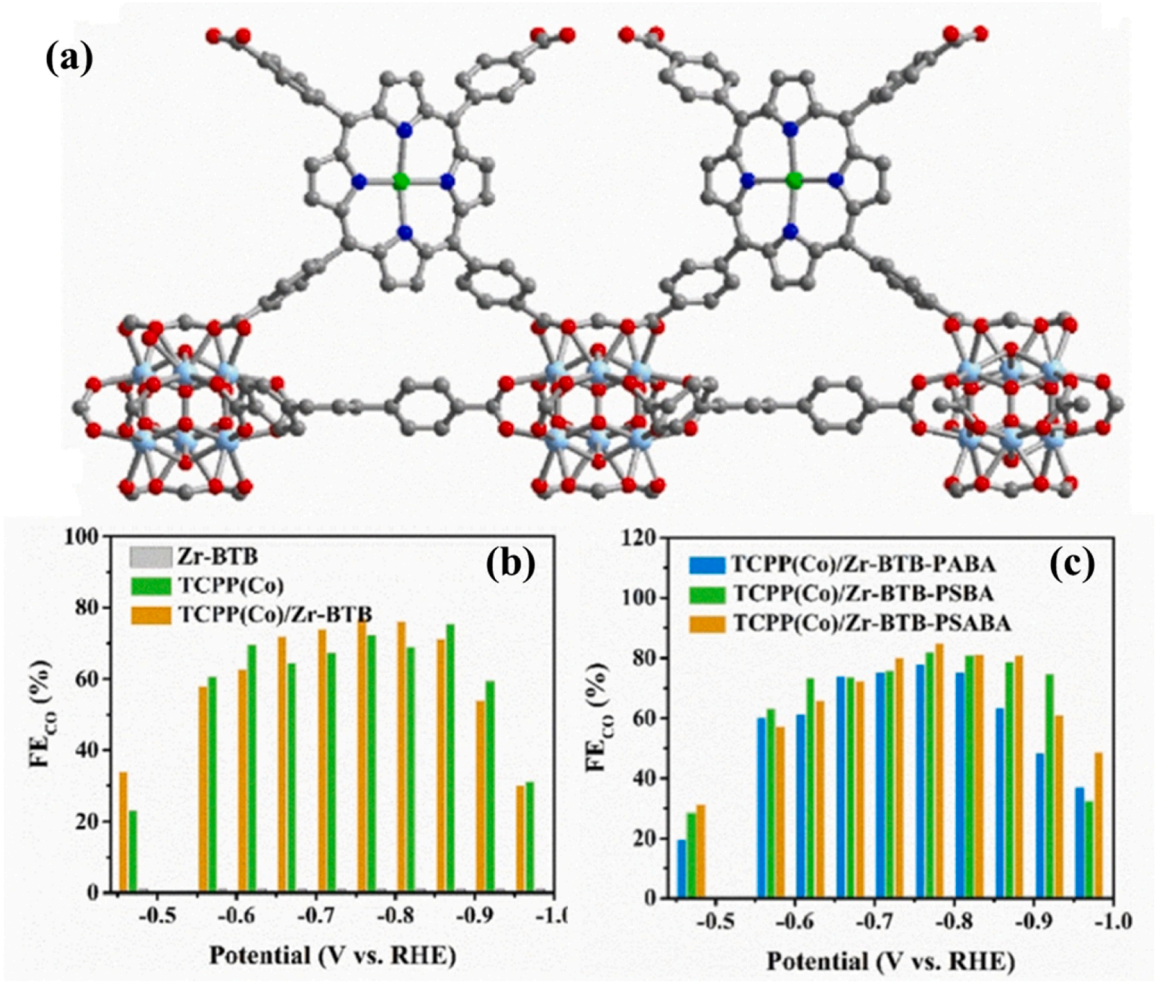


Fig. 9. (a) Crystal structure of TCPP(Co)/ZrBTB nanosheet. Gray is C, blue is N, red is O, bright green is Co, pale blue is Zr, and cyan is H; (b) and (c) CO Faradaic efficiency for different samples at different operating voltages. Reproduced with permission from ref. [165]; Copyright 2019 WILEY.

tunable architecture, facilitating catalytic reactions. In addition, MOFs contain metal cations and organic ligands that can operate as catalytic sites. Zn metal was recognized as a suitable alternative as a metal node for converting CO_2 into CO, owing to its cost and performance. Moreover, Zn-based MOFs have been utilized as electrocatalysts for CO_2 conversion. For instance, Wang and co-workers. successfully synthesized a zinc zeolitic imidazole framework (ZIF) from various precursors for electrocatalytic CO_2 reduction [166]. The results revealed that ZIF-8 formed from $ZnSO_4$ gave the highest yield for converting CO_2 into CO, with an FE of 65 %. The authors doubted that the Zn^{2+} sites have a crucial function in the catalytic reaction. Therefore, a Co-based MOF (ZIF-67) was prepared with an identical linker for comparison. CO was not detected in the ZIF-67 sample as an electrocatalyst. In addition, an appropriate solution of NaCl is also found for the CO_2 reduction process.

Another study demonstrated that the role of imidazole linker in ZIF structures is also essential in CO_2 conversion. Jiang et al. fabricated a series of ZIF structures with various linkers, including 2-methylimidazole, 2-nitroimidazole, benzimidazole, and 4-methyl-5-imidazolecarboxaldehyde, which resulted in the formation of ZIF-8, ZIF-108, ZIF-7, and SIM-1, respectively [167]. These materials were investigated for catalytic activity under identical conditions to estimate the role of imidazole linkers in CO_2 reduction. The results reveal that ZIF-8 with 2-methylimidazole displays the best yield for transforming CO_2 to CO with an FE of 81% (at −1.1 V vs. RHE), whereas ZIF-108 produces the largest CO current density of 12.8 mA cm^{-2} (at −1.3 V vs. RHE), as shown in Fig. 10a. The reaction mechanism was studied by computational chemistry using density function theory (DFT). The CO_2 molecule is predicted to be adsorbed on the C(sp^2) atoms of the imidazole linkers, as displayed in Fig. 10a-b. The free energy of *COOH on the Zn node is higher than that on the linker of ZIFs. The *COOH and *H adsorption free energies displayed in Fig. 10c-d explain why ZIF-8 is the best catalyst among the four materials for CO_2RR. ZIF-8 exhibits the lowest free energy of *H adsorption, implying that ZIF-8 has a high selectivity for CO_2 reduction.

4.3.2.2. Cobalt-based MOFs. Cobalt (Co) can exist in various reduction-oxidation states, including Co(I), Co(II), Co(III), and Co(IV). Therefore, Co-based materials are considered promising catalysts in the heterogeneous phase. Co-based MOFs have also been investigated for electrocatalysis like hydrogen production and CO_2 reduction. Because MOFs are inherently low conductivity materials, they are usually formed on conductive wafers involving fluorine-doped tin oxide (FTO), graphene, carbon paper, etc., that are used as electrodes in chemical reactions. For example, Kornienko et al. prepared a thin layer of $Al_2(OH)_2$TCPP-Co on FTO, which was utilized as a cathode for CO_2 reduction [168]. This catalyst displays a high selectivity for CO, with an FE of 76% (at −0.7 V vs. RHE). The proposed reaction mechanism determined that Co(I) created from one-electron reduction plays a role as a catalytic site in electrocatalytic CO_2RR. The formation of Co(I) active sites under reaction conditions and Tafel slope of 165 mV/decade reveals that the reaction mechanism can occur two cases: a CO_2 molecule adsorbs onto a Co(I) porphyrin coupled with a one-electron reduction or a one-electron

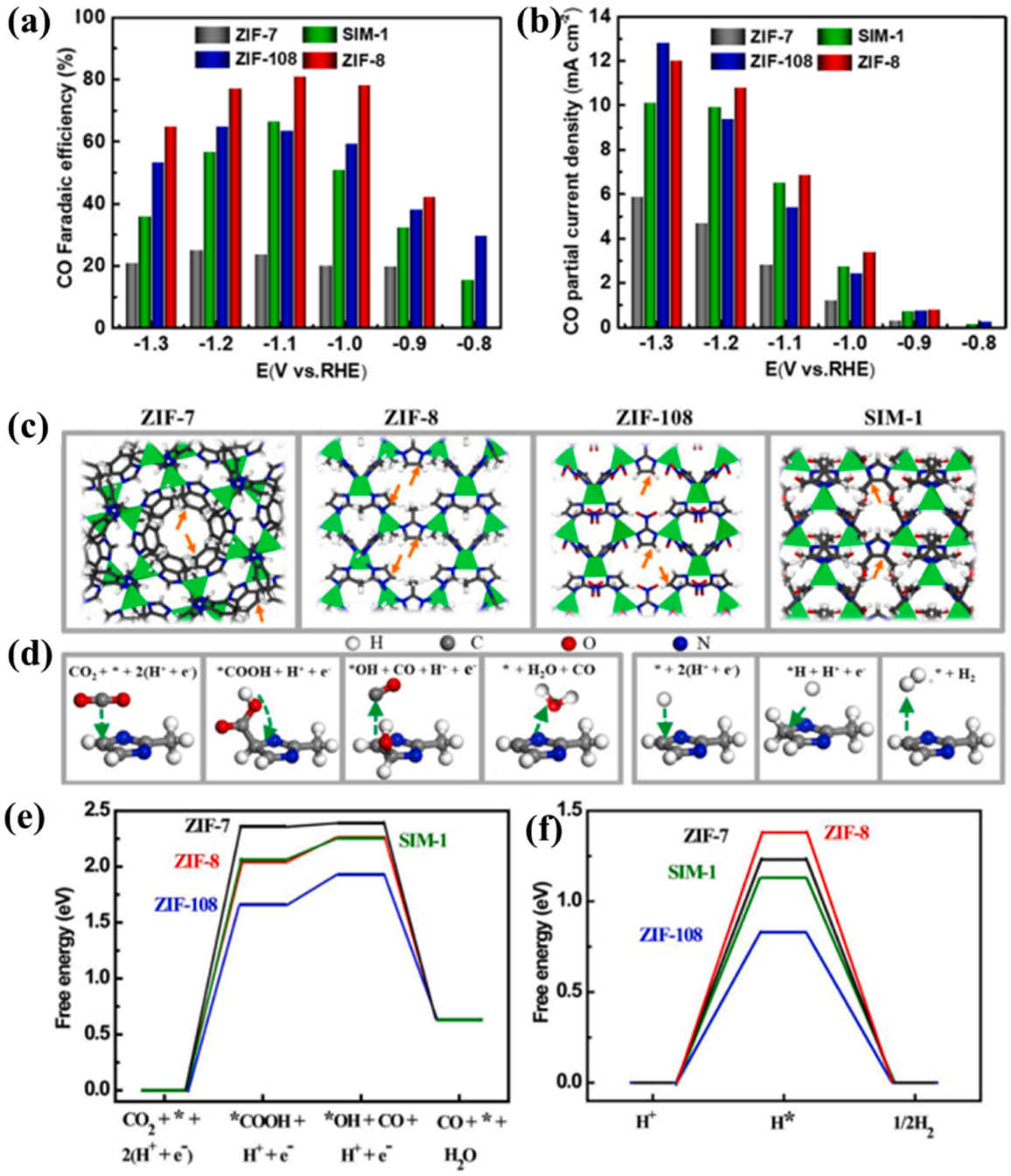


Fig. 10. The Faradaic efficiency (a) and current density (b) for CO product on ZIF-7, SIM-1, ZIF-108, and ZIF-8 at various potentials; (c) Most durable adsorption centers of *COOH on various imidazole linkers of ZIFs, which are marked by orange arrows; (d) Reaction mechanism on 2-methylimidazole linker; (e) Calculated free energy with solvent effect corrections for CO_2RR (e) and HER (f) by DFT method. Reproduced with permission from ref. [167]; Copyright 2018, Elsevier.

reduction of a Co(I) with CO_2 product.Recently, Huang et al. successfully fabricated a single crystal of NNU-15 for CO_2RR [169], as displayed in Fig. 11a. This material displays a very high selectivity of above 99% (at −0.6 V vs. RHE) for converting CO_2 into CO. In addition, the catalyst also shows high durability after testing for 110 h, as illustrated in Fig. 11b. The reaction mechanism suggests that CO_2 is adsorbed on Co sites and then converted to HCO_3^- through hydroxide ions (OH^-), whereas Co(I) operates as an electrocatalytic site for CO_2 reduction, as shown in Fig. 11c-d. This mechanism was confirmed by a computational simulation. The free energies of the transition states are illustrated in Fig. 11e.

4.3.2.3. Iron-based MOFs. Like cobalt-based MOFs, Fe-based MOFs have been recognized as efficient electrocatalysts in CO_2 reduction applications. For instance, Dong and co-workers introduced a composite of PCN-222(Fe)/C that was used as a catalyst for CO_2RR [170]. The crystal structure and morphology of PCN-222(Fe) are displayed in Fig. 12a-b. The results reveal that PCN-222(Fe)/C with a mass ratio of ½ is an optimal sample for electrocatalytic CO_2RR. This catalyst displays the highest FE_{CO} of 91 % in the first two h and is maintained at a high FE_{CO} after testing for ten hours, as shown in Fig. 12c. In addition, Fig. 12d implies that the electrode is stable for 10 testing hours. Another study based on Fe-based MOF was provided by Hod et al. [171]. Fe-MOF-525 was grown on FTO, which was used as a cathode for CO_2 conversion.

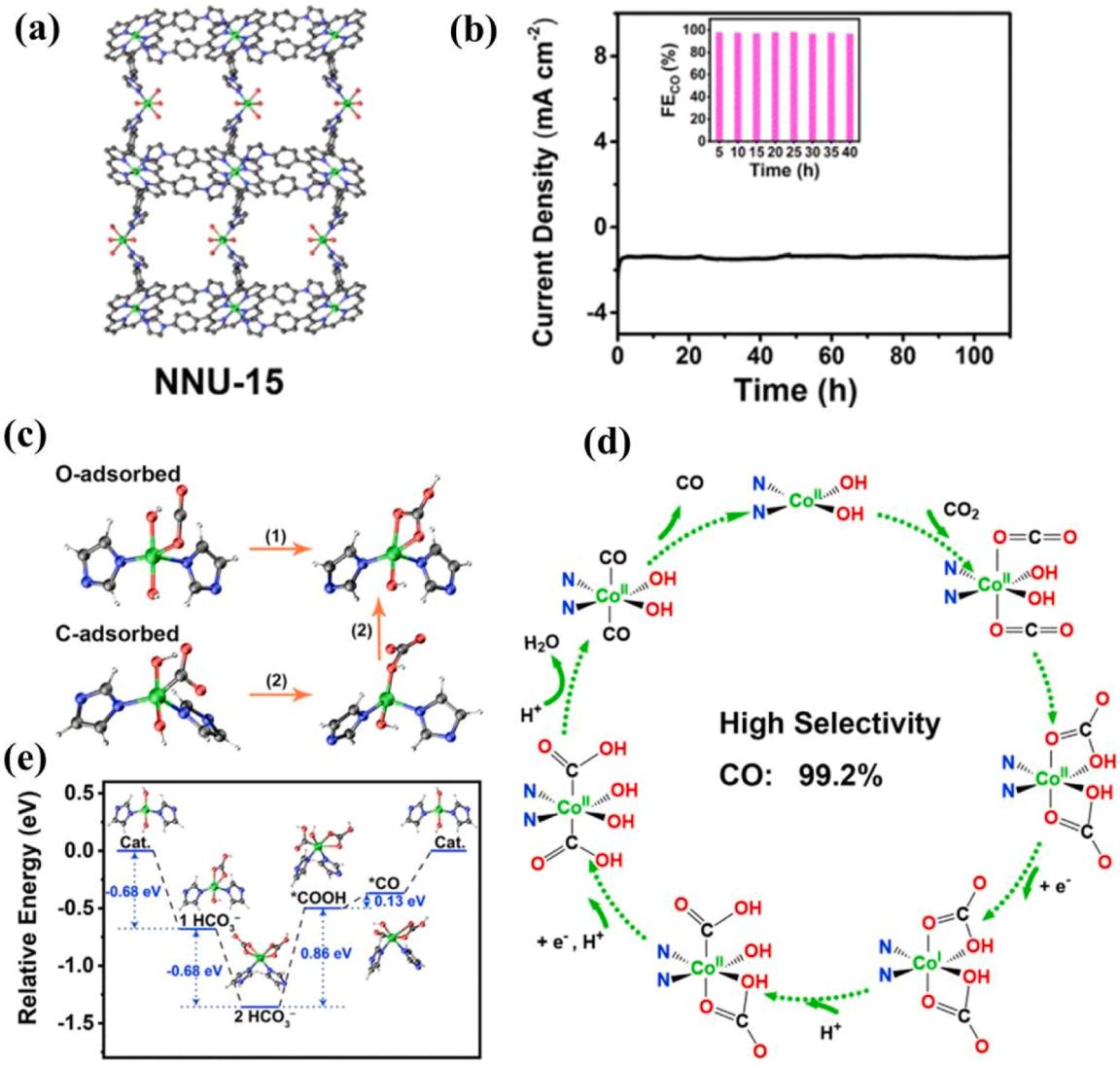


Fig. 11. (a) Crystal structure of NNU-15; (b) Stability test of NNU-15 at a fixed potential of −0.6 V (vs. RHE); (c) Structural illustration for the adsorption of CO_2 on Co(II) site; (d) Reaction mechanism of CO_2 conversion into CO; (e) The corresponding free energies for each step in CO_2RR. Reproduced with permission from ref. [169]; Copyright 2019, Elsevier.

This catalyst exhibits an FE of 54 % for CO and 45 % for H_2 in the absence of 2,2,2-trifluoroethanol (TFE). FE_{CO} is promoted from 54 % to 60 % with TFE in the electrolyte.

4.3.3. MOF-derived composites as electrocatalysts

Pristine MOFs have been scrutinized for the transformation of CO_2 to valuable chemicals, as mentioned above. However, the low charge conduction restricts their application in electrocatalytic reactions. Therefore, many approaches have been developed to alter MOF's properties for increased catalytic activity. In terms of electrocatalytic CO_2RR, MOFs have also been utilized as initial molecules to create composites for efficient catalysis. In particular, they could be combined into the adjustable pores of MOF structures or bounded by MOF sheets to fabricate MOF composites with core-shell architectures, which expeditiously impede the loss of active centers [172].

4.3.3.1. MOF-derived metal nanoparticles. Cu is an extremely desirable catalyst for CO_2 conversion due to its availability, inexpensive and the ability to produce several chemicals. The role of the morphology of Cu-related electrodes is significant in CO_2 conversion by the electrochemical process with high selectivity. In particular, Cu nanoparticles with few nanometer sizes are very desirable for electrocatalytic CO_2 reduction because of their resistant to electrochemically caused aggregation. Hupp et al. reported on the results of a thin layer of NU-1000 uniformly interspersed with Cu^{2+} centers via a solution-phase analog of atomic layer deposition in MOFs (SIM). Metallic Cu NPs were formed by electrochemical reduction of Cu in the film inhibited by the networks of the MOF, following in an electroactive Cu-SIM NU1000 thin layer for CO_2 conversion [172].

In one study, Luna et al. illustrate an exciting work by using Au nanoarchitecture microelectrodes (AuNMEs) as a template to deposit various MOF materials through two-step of layer-layer and solvothermal technique toward CO_2 conversion. The result indicated the usage of MOF prevents the formation of CO and generates a little content of methane and ethane on AuNMEs. Besides, the CO creation can be detected when a voltage of −1.0 V (vs. RHE) was applied for the electrochemical system, which was attribute to the MOF decomposition [173].

4.3.3.2. Metal nanoparticles/MOF hybrid structure. Buonsanti et al. fabricated a hybrid structure of Ag@Al-PMOF for CO_2 conversion by the electrocatalytic method [174]. The as-synthesized Ag@Al-PMOF

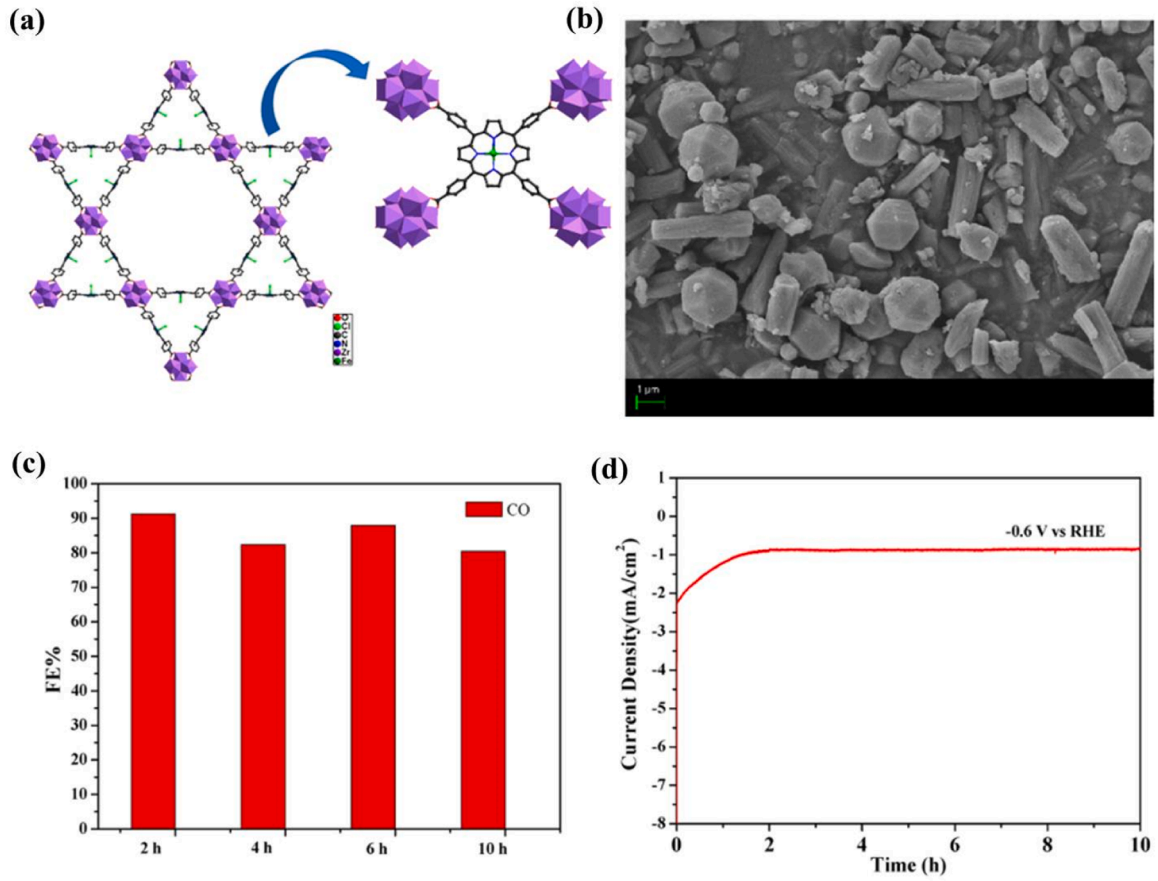


Fig. 12. (a) A crystal structure of PCN-222(Fe); (b) SEM image of PCN-222(Fe); (c) The Faradaic efficiency for CO product of PCN-222(Fe)/C; (d) Stability test of Co-PMOF at a fixed potential of −0.6 V (vs. RHE). Reproduced with permission from ref. [170]; Copyright 2018, American Chemical Society.

architecture exhibited about two times higher than that of Ag alone to transform CO_2 into carbon monoxide and a drastic reduction in hydrogen production. Consequently, the Ag/Al-PMOF interface showed a very enhanced catalytic performance. The synthetic tunability boosts the transport of charge from MOF structure to nanocrystals, while the mass transport was improved by the porous structure of MOF film.

In addition to anchoring metal NPs, another approach to address the low electron-donating ability and electronic conductivity of MOFs was illustrated by Lan et al., where an implanted metallocene (MCp2) was utilized as a promising electron donor and transporter to enhance the charge density of the MOF architecture. As a result, MCp_2@MOF-545-Co shows a high yield for CO_2 conversion by electrochemical technique. In Particular, $CoCp_2$@MOF545-Co gave a high selectivity for converting CO_2 to CO with an FE of 97 % at −0.7 V vs. RHE.

4.4. MOFs for CO_2 conversion into formate, formic acid, alcohols, and hydrocarbons

4.4.1. MOFs for CO_2 conversion into formate, formic acid

Hinogami et al. synthesized and estimated the catalytic performance of copper rubeanate MOF (CR-MOF) in CO_2RR [175]. This work reveals that CR-MOF exhibits a high selectivity for the formation of HCOOH with a speed of 13.4 μmol/cm^2/h, which is 13 times faster than that of the Cu electrode. The reason for this being that the electron density of CR-MOF is lower than that of Cu metal, leading to the weak interaction between CO_2 and CR-MOF, which facilitates the formation of HCOOH. Another study on Cu-based MOFs was reported by Kumar for the selective electroreduction of carbon-dioxide to form oxalic acid [176]. The authors scrutinized the influence of the solvent on the performance of $Cu_3(BTC)_2$ for CO_2 reduction. HCOOH was formed with a high purity of 90 %, and FE was 51 % in a mixture of N, N-dimethylformamide (DMF) and tetrabutylammonium tetrafluoroborate (TBATFB) (Fig. 13). The improved yield is attributed to the formation of Cu(I) centers, facilitating the generation of HCOOH. The reaction mechanism suggests that $HCOO^-$ is created from the dimerization process of $CO_2^{\bullet-}$, taking a proton from DMF to generate HCOOH. Bi-based MOFs were also explored in electro-reduction of CO_2 to formate. For instance, Lamagni and co-workers convert Bi(btb) into Bi nanoparticles as efficient catalysts for $HCOO^-$ generation [143]. This material exhibited an excellent catalytic activity with very high FE (approximately 95%), which was ascribed to the well-dispersion Bi in the organic framework.

Recently, a new MOF of MFM-300(In) was grown on an In foil by the electrochemical method for the electrocatalytic CO_2 conversion [177]. The work indicated that MFM-300(In)/In displayed a high-performance (FE_{HCOOH} of 91.1%) and outstanding durability. This account also revealed that MFM-300(In)/In gives better catalytic activity than MFM-300(In)/carbon paper. The result was attributed to the excellent contact between MOF and In substrated in the synthetic process.

4.4.2. MOFs for CO_2 conversion into alcohols and hydrocarbons

Alcohols, including ethanol and methanol, were evaluated as high energy density fuels. The reduction of CO_2 by MOF-catalysts is a promising pathway to produce the alcohols because of its facial experiment process. Cathode made from Cu-based MOFs is usually utilized toward the conversion of CO_2 into methanol or ethanol. For example, Albo et al. investigated the catalytic activity of various Cu-MOFs for CO_2 reduction [178]. The study revealed that HKUST-1 showed the highest performance with a FE of 15.9 % for methanol and ethanol formation. Later, they improved CO_2 reduction performance by mixing HKUST-1 with a Bi-based MOF (CAU-17) [179]. The authors found that the

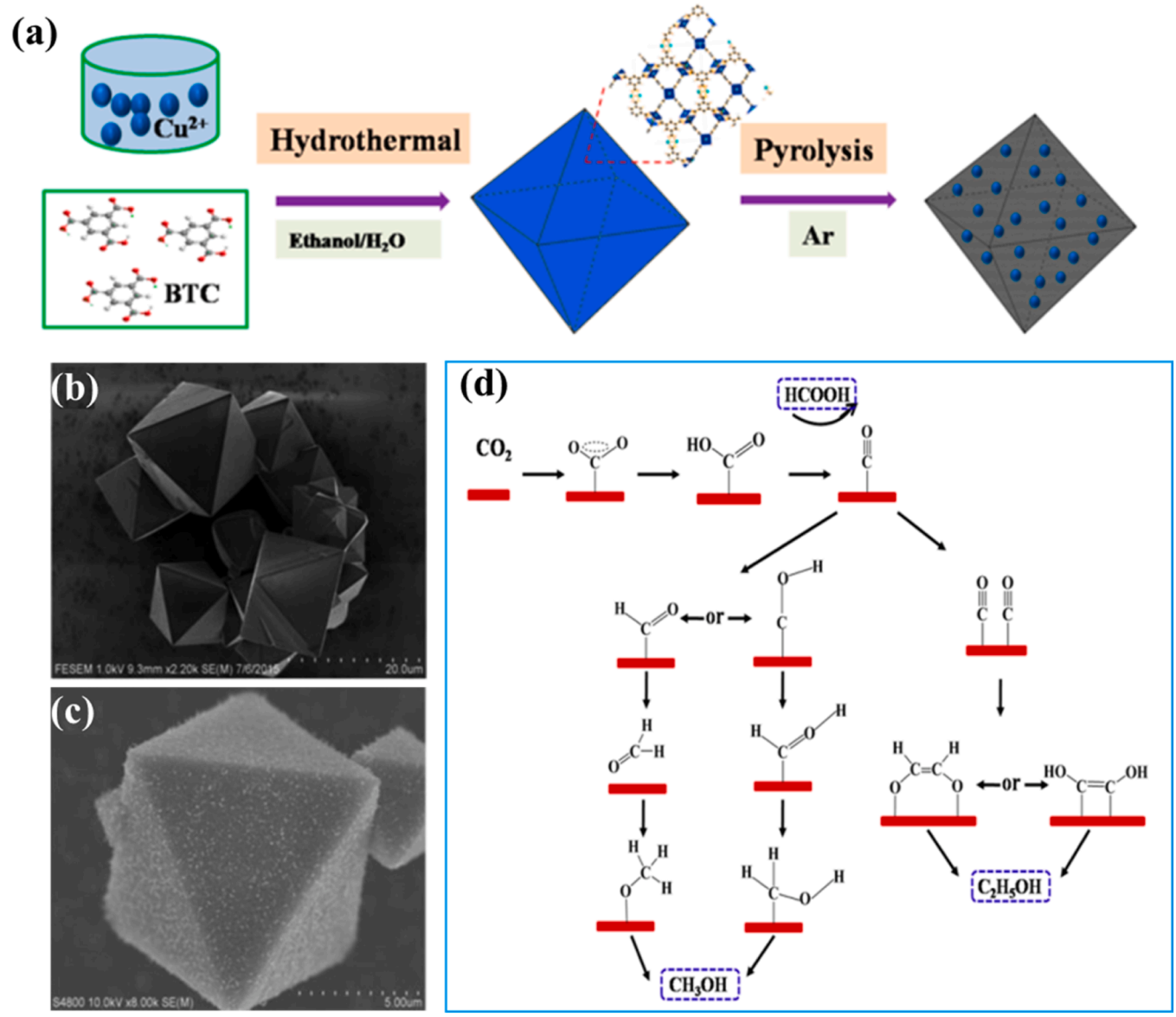


Fig. 13. (a) Graphical diagram of the preparation of Cu-BTC and 0D Cu/C-1000; (b) SEM image of Cu-BTC; (c) SEM image of 0D Cu/C-1000; (d) Proposed mechanism for electrocatalytic CO_2RR on 0D Cu/C-1000. Reproduced with permission from ref.[184]; Copyright 2017, American Chemical Society.

optimal sample exhibited a high $FE_{alcohols}$ of 36.9%. The reason for this being that Cu/Bi-MOF created a synergic influence, which plays a vital role in facilitating interaction between active moieties and transition states. Perfecto-Irigaray and co-workers reported another work related to the HKUST-1 for CO_2 transformation [180]. Various metals doping (Pd, Zn, and Ru) was conducted to improve the electrocatalytic activity of HKUST-1. The authors found that Ru-doped HKUST-1 exhibited the best activity with a FE of 47.2 % for methanol and ethanol. However, its performance was reduced above three times after an hour of operation.

On the other hand, methane and ethylene were also considered as useful compounds in particular applications. To date, using MOFs as electrocatalysts to transform CO_2 to hydrocarbons is still limited. Recently, Yang et al. illustrated a potential MOF in the reduction of CO_2 to methane and ethylene [144]. Cu nanoparticles were created from Cu^{II}/ade-MOFs, play as active centers for CO_2 reduction to CH_4 and C_2H_4. In addition, Li and co-workers studied the formation of methane using molecular lignad called N-heterocyclic carbene molecules(NHCs) [181]. This lignad have a ring structure with one nitrogen (N) atom and one divalent carbon (C) atom in a six-electron valance shell. Copper SAS (2Bn-Cu) was combined with NHC linker to produce methane with FE upto 81 %. The NHC acted as a reduction catalytic center by anchoring the Cu SAS via the metal carbon bond. Also, the adsorption of CHO* intermediate can be increased due to the electron donator effect of NHC.

Overall, the generation of various products depends on the natural properties of metal sites and organic linkers. Notably, Zn -, Co -, Ni, and Fe-based MOFs have been recognized as promising materials for CO_2 transformation to CO, whereas Cu-, Bi-based MOFs facilitate the transformation of CO_2 to formate, formic acid, alcohol, and hydrocarbons. The reaction mechanisms were also proposed in a large number of studies, which were based on the calculation Gibb energy of intermediates. Besides, the role of linkers is incredibly significant in CO_2 reduction. For example, various linkers, including 2-methylimidazole, 2-nitroimidazole, benzimidazole, and 4-methyl-5-imidazolecarboxaldehyde was utilized to prepare the different ZIFs for CO_2 reduction application by electrochemical method [167]. The study revealed that the imidazolate linkers play a crucial role in the adsorption of intermediate species. Especially, 2-methylimidazole gave the lowest total free energy on the proposed-reaction pathway. As a result, ZIF-8 constructed from 2-methylimidazole displayed the highest FE for CO_2 conversion into CO. Moreover, electrolyte also influences the selectivity

of product. As a case in point, six various electrolytes, involving TBAB/DMF (TBAB = tetrabutylammonium bromide; DMF = dimethylformamide), TBAP/CH_3OH (TBAB = tetrabutylammonium perchlorate), CH_3COOK/CH_3OH, $KHCO_3/H_2O$, TBAB/CH_3OH, KBr/CH_3OH was evaluated for the catalytic activity of Cu-MOF/GO for CO_2 transformation into HCOOH [142]. Authors found that TBAB/DMF shows the largest FE_{HCOOH} (58%), whereas CH_3COOK/CH_3OH gave the lowest FE_{HCOOH} (15%).

5. Conclusion and outlook

In this review current progresses made in the electrocatalytic CO_2RR were investigated with their corresponding examples. The utilization of layered double hydroxides (LDHs) and metal-organic frameworks (MOFs) as electrocatalysts for CO_2 reduction holds tremendous promise for addressing the pressing challenges of climate change and energy sustainability. Throughout this review, we have explored the fundamental properties, synthesis methods, and electrocatalytic performance of LDHs and MOFs in CO_2 reduction reactions. LDHs, with their layered structure and tunable composition, offer high surface area, abundant active sites, and excellent ion conductivity, making them highly attractive for CO_2 electrocatalysis. Similarly, MOFs exhibit remarkable structural diversity, pore size controllability, and metal ion variability, enabling tailored design and enhanced catalytic activity for CO_2 reduction.

Advancements in LDH- and MOF-based electrocatalysis has revealed exciting opportunities for improving CO_2 conversion efficiency, selectivity, and stability. LDHs have demonstrated impressive catalytic performance in CO_2 reduction, with notable achievements in enhancing electron transfer kinetics, optimizing active site density, and mitigating side reactions. Studies have shown that, even if a lot of developments have been made, the efficiency and selectivity of the MOF catalyst are low and need further improvement. Several approaches include core-shell nanostructure, MOF/carbon material composite, and confinement engineering conducted to accelerate CO_2RR efficiency. First, the core-shell nanostructure is a potential strategy for obtaining high selectivity in CO_2RR. Because it illustrates a useful way to regulate the electronic properties of the surface environment, facilitating the adsorption of intermediates in the catalytic process. Second, the combination of MOFs with carbon materials (graphene oxide, carbon nanotubes) is a facial approach for producing high-performance CO_2RR catalysts due to boosted electron transfer. In terms of confinement engineering. The metal ions and organic linkers existing on MOFs may effectively confine single or dual metallic atoms as high active centers through a facial annealing process [182,183]. As a result, the performance of the catalytic reaction is enhanced. Moreover, the development of catalysts with high selectivity of organic small molecules and products having long carbon chains still is a challenging task.

For excellent electrocatalytic CO_2RR performance, advancements can be made by addressing these two areas of research. Looking for catalysts with unique structures, properties and compositions must remain to be the priority in electro and photoreduction of CO_2 investigation. Researches directed by theoretical calculation are an influential tool for producing and studying newly found catalysts by relating the overpotentials needed for the reaction intermediates and energy barriers available. In addition, recent techno-economic analyses have proposed lower limits of FE and partial current density for desired product. To commercialize CO_2RR technologies, rational reactor design with high-performance catalysts utilizing gas-phase CO_2 reactant must be preceded.

CRediT authorship contribution statement

Mahider Asmare Tekalgne: Writing – original draft, Data curation. **Ha Huu Do:** Writing – original draft, Data curation. **Gyeong Ho Han:** Writing – original draft, Data curation. **Sung Hyun Hong:** Methodology. **Jin Hyuk Cho:** Methodology. **Sang Hyun Ahn:** Writing – review & editing, Supervision. **Soo Young Kim:** Writing – review & editing, Supervision, Conceptualization.

Declaration of competing interest

The authors declare that they have no known competing financial interests or personal relationships that could have appeared to influence the work reported in this paper.

Data availability

The authors do not have permission to share data.

Acknowledgments

This research was supported by the NRF funded by the Korean government [2022M3H4A1A01012712].

References

[1] JR. Li, Y. Ma, M.C. McCarthy, J. Sculley, J. Yu, HK. Jeong, P.B. Balbuena, HC. Zhou, Carbon dioxide capture-related gas adsorption and separation in metal-organic frameworks, Coord. Chem. Rev. 255 (15–16) (2011) 1791–1823.
[2] S. Xiang, Y. He, Z. Zhang, H. Wu, W. Zhou, R. Krishna, B. Chen, Microporous metal-organic framework with potential for carbon dioxide capture at ambient conditions, Nat. Commun. 3 (2012) 954.
[3] T. Grant, A. Guinan, C.Y. Shih, S. Lin, D. Vikara, D. Morgan, D. Remson, Comparative analysis of transport and storage options from a CO_2 source perspective, Int. J. Greenhouse Gas Control 72 (2018) 175–191.
[4] D.Y. Leung, G. Caramanna, M.M. Maroto-Valer, An overview of current status of carbon dioxide capture and storage technologies, Renew. Sustain. Energy Rev. 39 (2014) 426–443.
[5] D. Vikara, C.Y. Shih, S. Lin, A. Guinan, T. Grant, D. Morgan, D. Remson, US DOE's economic approaches and resources for evaluating the cost of implementing carbon capture, utilization, and storage (CCUS), J. Energy Eng. 5 (4) (2017) 307–340.
[6] M. Chhowalla, H.S. Shin, G. Eda, LJ. Li, K.P. Loh, H. Zhang, The chemistry of two-dimensional layered transition metal dichalcogenide nanosheets, Nat. Chem. 5 (4) (2013) 263.
[7] Y. Tan, W. Nookuea, H. Li, E. Thorin, J. Yan, Property impacts on carbon capture and storage (CCS) processes: a review, Energy Convers. Manage. 118 (2016) 204–222.
[8] M. Halmann, Photoelectrochemical reduction of aqueous carbon dioxide on p-type gallium phosphide in liquid junction solar cells, Nature 275 (5676) (1978) 115–116.
[9] T. Inoue, A. Fujishima, S. Konishi, K. Honda, Photoelectrocatalytic reduction of carbon dioxide in aqueous suspensions of semiconductor powders, Nature 277 (5698) (1979) 637–638.
[10] W. Wang, S. Wang, X. Ma, J. Gong, Recent advances in catalytic hydrogenation of carbon dioxide, Chem. Soc. Rev. 40 (7) (2011) 3703–3727.
[11] J.W. Maina, C. Pozo-Gonzalo, L. Kong, J. Schütz, M. Hill, L.F. Dumée, Metal organic framework based catalysts for CO_2 conversion, Mater. Horiz. 4 (3) (2017) 345–361.
[12] M. Melchionna, P. Fornasiero, Updates on the Roadmap for Photocatalysis, ACS. Catal. 10 (10) (2020) 5493–5501.
[13] S. Nitopi, E. Bertheussen, S.B. Scott, X. Liu, A.K. Engstfeld, S. Horch, B. Seger, I. E. Stephens, K. Chan, C. Hahn, Progress and perspectives of electrochemical CO_2 reduction on copper in aqueous electrolyte, Chem. Rev. 119 (12) (2019) 7610–7672.
[14] Z. Gu, H. Shen, Z. Chen, Y. Yang, C. Yang, Y. Ji, Y. Wang, C. Zhu, J. Liu, J. Li, Efficient electrocatalytic CO_2 reduction to C^{2+} alcohols at defect-site-rich Cu surface, Joule 5 (2) (2021) 429–440.
[15] M. Royer, Réduction de l'acide carbonique en acide formique, Compt. Rend 1870 (1870) 731–732.
[16] J. Augustynski, P. Kedzierzawski, B. Jermann, Electrochemical reduction of CO_2 at metallic electrodes, Stud. Surf. Sci. Catal. (1998) 107–116.
[17] Y. Hori, H. Wakebe, T. Tsukamoto, O. Koga, Electrocatalytic process of CO selectivity in electrochemical reduction of CO_2 at metal electrodes in aqueous media, Electrochim. Acta 39 (11–12) (1994) 1833–1839.
[18] S. Ponnurangam, I.V. Chernyshova, P. Somasundaran, Nitrogen-containing polymers as a platform for CO_2 electroreduction, Adv. Colloid Interface Sci. 244 (2017) 184–198.
[19] J.T. Feaster, C. Shi, E.R. Cave, T. Hatsukade, D.N. Abram, K.P. Kuhl, C. Hahn, J. K. Nørskov, T. Jaramillo, Understanding selectivity for the electrochemical reduction of carbon dioxide to formic acid and carbon monoxide on metal electrodes, ACS. Catal. 7 (7) (2017) 4822–4827.

[20] A. Bagger, W. Ju, A.S. Varela, P. Strasser, J. Rossmeisl, Electrochemical CO_2 reduction: a classification problem, Chemphyschem. 18 (22) (2017) 3266–3273.
[21] M. Jouny, W. Luc, F. Jiao, High-rate electroreduction of carbon monoxide to multi-carbon products, Nat. Catal. 1 (10) (2018) 748–755.
[22] C. Zhan, F. Dattila, C. Rettenmaier, A. Bergmann, S. Kühl, R. García-Muelas, N. r. López, B.R. Cuenya, Revealing the co coverage-driven C–C coupling mechanism for electrochemical CO_2 reduction on Cu_2O nanocubes via operando Raman spectroscopy, ACS. Catal. 11 (13) (2021) 7694–7701.
[23] Z.W. Seh, J. Kibsgaard, C.F. Dickens, I. Chorkendorff, J.K. Nørskov, T. Jaramillo, Combining theory and experiment in electrocatalysis: insights into materials design, Science (1979) 355 (6321) (2017).
[24] X. Liu, L. Dai, Carbon-based metal-free catalysts, Nature 1 (11) (2016) 1–12.
[25] X. Duan, C. Wang, A. Pan, R. Yu, X. Duan, Two-dimensional transition metal dichalcogenides as atomically thin semiconductors: opportunities and challenges, Chem. Soc. Rev. 44 (24) (2015) 8859–8876.
[26] C. Tan, H. Zhang, Two-dimensional transition metal dichalcogenide nanosheet-based composites, Adv. Mater. 44 (9) (2015) 2713–2731.
[27] B. Anasori, M.R. Lukatskaya, Y. Gogotsi, 2D metal carbides and nitrides (MXenes) for energy storage, Nat. Rev. Mater. 2 (2) (2017) 16098.
[28] R. Ma, T. Sasaki, Nanosheets of oxides and hydroxides: ultimate 2D charge-bearing functional crystallites, Adv. Mater. 22 (45) (2010) 5082–5104.
[29] H. Kang, IK. Park, Reconstruction and intercalating anion exchange of ZnAl-layered double hydroxide, Ceram. Int. 48 (3) (2022) 3030–3036.
[30] HC. Zhou, J.R. Long, O.M. Yaghi, Introduction to metal–organic frameworks, Chem. Rev. 112 (2) (2012) 673–674.
[31] X. Li, J. Wen, J. Low, Y. Fang, J. Yu, Design and fabrication of semiconductor photocatalyst for photocatalytic reduction of CO_2 to solar fuel, Sci. China Mater. 57 (1) (2014) 70–100.
[32] Y. Ma, X. Wang, Y. Jia, X. Chen, H. Han, C. Li, Titanium dioxide-based nanomaterials for photocatalytic fuel generations, Chem. Rev. 114 (19) (2014) 9987–10043.
[33] D.A. Gómez-Gualdrón, T.C. Wang, P. García-Holley, R.M. Sawelewa, E. Argueta, R.Q. Snurr, J.T. Hupp, T. Yildirim, O.K. Farha, Understanding volumetric and gravimetric hydrogen adsorption trade-off in metal–organic frameworks, ACS Appl. Mater. Interfaces 9 (39) (2017) 33419–33428.
[34] S. Øien-Ødegaard, B. Bouchevreau, K. Hylland, L. Wu, R. Blom, C. Grande, U. Olsbye, M. Tilset, K.P. Lillerud, UiO-67-type metal–organic frameworks with enhanced water stability and methane adsorption capacity, Inorg. Chem 55 (5) (2016) 1986–1991.
[35] D.K. Maity, A. Halder, B. Bhattacharya, A. Das, D. Ghoshal, Selective CO_2 adsorption by nitro functionalized metal organic frameworks, Cryst. Growth Des. 16 (3) (2016) 1162–1167.
[36] J. Duan, S. Chen, C. Zhao, Ultrathin metal-organic framework array for efficient electrocatalytic water splitting, Nat. Commun. 8 (1) (2017) 1–7.
[37] W. Wang, X. Xu, W. Zhou, Z. Shao, Recent progress in metal-organic frameworks for applications in electrocatalytic and photocatalytic water splitting, Adv. Sci. 4 (4) (2017) 1600371.
[38] G. Zhong, D. Liu, J. Zhang, The application of ZIF-67 and its derivatives: adsorption, separation, electrochemistry and catalysts, J. Mater. Chem. A 6 (5) (2018) 1887–1899.
[39] X. Xiao, S. Zheng, X. Li, G. Zhang, X. Guo, H. Xue, H. Pang, Facile synthesis of ultrathin Ni-MOF nanobelts for high-efficiency determination of glucose in human serum, J. Mater. Chem. B 5 (26) (2017) 5234–5239.
[40] Y. Sun, Y. Li, N. Wang, Q.Q. Xu, L. Xu, M. Lin, Copper-based metal-organic framework for non-enzymatic electrochemical detection of glucose, Electroanalysis. 30 (3) (2018) 474–478.
[41] P. Kumar, A. Deep, KH. Kim, Metal organic frameworks for sensing applications, Trends Anal. Chem. 73 (2015) 39–53.
[42] P. Horcajada, C. Serre, M. Vallet-Regí, M. Sebban, F. Taulelle, G. Férey, Metal–organic frameworks as efficient materials for drug delivery, Angew. Chem. Int. Ed. 45 (36) (2006) 5974–5978.
[43] M.A. Tekalgne, H. Do, A. Hasani, Q. Van Le, H. Jang, S. Ahn, S. Kim, Two-dimensional materials and metal-organic frameworks for the CO_2 reduction reaction, Mater. Today Adv. 5 (2020) 100038.
[44] A.J. Clough, J.W. Yoo, M.H. Mecklenburg, S.C. Marinescu, Two-dimensional metal–organic surfaces for efficient hydrogen evolution from water, J. Am. Chem. Soc. 137 (1) (2015) 118–121.
[45] R. Dong, Z. Zheng, D.C. Tranca, J. Zhang, N. Chandrasekhar, S. Liu, X. Zhuang, G. Seifert, X. Feng, Immobilizing molecular metal dithiolene–diamine complexes on 2D metal–organic frameworks for electrocatalytic H_2 production, ChemEur. J. 23 (10) (2017) 2255–2260.
[46] Y.P. Wu, W. Zhou, J. Zhao, W.W. Dong, Y.Q. Lan, D.S. Li, C. Sun, X. Bu, Surfactant-assisted phase-selective synthesis of new cobalt MOFs and their efficient electrocatalytic hydrogen evolution reaction, Angew. Chem. Int. Ed. 56 (42) (2017) 13001–13005.
[47] X. Zhao, B. Pattengale, D. Fan, Z. Zou, Y. Zhao, J. Du, J. Huang, C. Xu, Mixed-node metal–organic frameworks as efficient electrocatalysts for oxygen evolution reaction, ACS. Energy Lett. 3 (10) (2018) 2520–2526.
[48] B.A. Johnson, A. Bhunia, S. Ott, Electrocatalytic water oxidation by a molecular catalyst incorporated into a metal–organic framework thin film, Dalton. Trans. 46 (5) (2017) 1382–1388.
[49] Z. Xue, K. Liu, Q. Liu, Y. Li, M. Li, CY. Su, N. Ogiwara, H. Kobayashi, H. Kitagawa, M. Liu, Missing-linker metal-organic frameworks for oxygen evolution reaction, Nat. Commun. 10 (1) (2019) 1–8.
[50] J. Jiang, L. Huang, X. Liu, L. Ai, Bioinspired cobalt–citrate metal–organic framework as an efficient electrocatalyst for water oxidation, ACS Appl. Mater. Interfaces 9 (8) (2017) 7193–7201.
[51] C. Liu, W. Wang, B. Liu, J. Qiao, L. Lv, X. Gao, X. Zhang, D. Xu, W. Liu, J. Liu, Recent advances in MOF-based nanocatalysts for photo-promoted CO2 reduction applications, 9(8) (2019), pp. 658.
[52] D. Narváez-Celada, A.S. Varela, CO_2 electrochemical reduction on metal–organic framework catalysts: current status and future directions, J. Mater. Chem. 10 (11) (2022) 5899–5917.
[53] X. Wang, M. Fan, Y. Guan, Y. Liu, M. Liu, T.N. Karsili, J. Yi, XD. Zhou, J. Zhang, MOF-based electrocatalysts for high-efficiency CO_2 conversion: structure, performance, and perspectives, J. Mater. Chem. 9 (40) (2021) 22710–22728.
[54] X. Li, QL. Zhu, MOF-based materials for photo-and electrocatalytic CO_2 reduction, EnergyChem 2 (3) (2020) 100033.
[55] D. Li, M. Kassymova, X. Cai, SQ. Zang, HL. Jiang, Photocatalytic CO_2 reduction over metal-organic framework-based materials, Coord. Chem. Rev. 412 (2020) 213262.
[56] Y. Zhao, L. Zheng, D. Jiang, W. Xia, X. Xu, Y. Yamauchi, J. Ge, J. Tang, Nanoengineering metal–organic framework-based materials for use in electrochemical CO_2 reduction reactions, Small. 17 (16) (2021) 2006590.
[57] R.R. Ikreedeegh, M. Tahir, A critical review in recent developments of metal-organic-frameworks (MOFs) with band engineering alteration for photocatalytic CO_2 reduction to solar fuels, J. CO_2 Util. 43 (2021) 101381.
[58] L. Zhang, J. Zhang, Metal-organic frameworks for CO_2 photoreduction, Front. Energy 13 (2) (2019) 221–250.
[59] I.I. Alkhatib, C. Garlisi, M. Pagliaro, K. Al-Ali, G. Palmisano, Metal-organic frameworks for photocatalytic CO_2 reduction under visible radiation: a review of strategies and applications, Catal. Today 340 (2020) 209–224.
[60] XY. Dao, WY. Sun, Single-and mixed-metal–organic framework photocatalysts for carbon dioxide reduction, Inorg. Chem. Front. 8 (13) (2021) 3178–3204.
[61] X. Feng, Y. Pi, Y. Song, C. Brzezinski, Z. Xu, Z. Li, W. Lin, Metal–organic frameworks significantly enhance photocatalytic hydrogen evolution and CO_2 reduction with earth-abundant copper photosensitizers, J. Am. Chem. Soc. 142 (2) (2020) 690–695.
[62] P.M. Stanley, J. Haimerl, C. Thomas, A. Urstoeger, M. Schuster, N.B. Shustova, A. Casini, B. Rieger, J. Warnan, R. Fischer, Host–guest interactions in a metal–organic framework isoreticular series for molecular photocatalytic CO_2 reduction, Angew. Chem. Int. Ed. 60 (33) (2021) 17854–17860.
[63] Y. Fu, D. Sun, Y. Chen, R. Huang, Z. Ding, X. Fu, Z. Li, An amine-functionalized titanium metal–organic framework photocatalyst with visible-light-induced activity for CO_2 reduction, Angew. Chem. Int. Ed. 51 (14) (2012) 3364–3367.
[64] F. Guo, YP. Wei, SQ. Wang, XY. Zhang, FM. Wang, WY. Sun, Pt nanoparticles embedded in flowerlike NH_2-UiO-68 for enhanced photocatalytic carbon dioxide reduction, J. Mater. Chem. A 7 (46) (2019) 26490–26495.
[65] D.L.T. Nguyen, C.W. Lee, J. Na, MC. Kim, N.D.K. Tu, S.Y. Lee, Y.J. Sa, D.H. Won, HS. Oh, H. Kim, Mass transport control by surface graphene oxide for selective CO production from electrochemical CO_2 reduction, ACS. Catal. (2020).
[66] J. Greeley, T.F. Jaramillo, J. Bonde, I. Chorkendorff, J.K. Nørskov, Computational high-throughput screening of electrocatalytic materials for hydrogen evolution, Nat. Mater. 5 (11) (2006) 909–913.
[67] W.J. Durand, A.A. Peterson, F. Studt, F. Abild-Pedersen, J.K. Nørskov, Structure effects on the energetics of the electrochemical reduction of CO_2 by copper surfaces, Surf. Sci. 605 (15–16) (2011) 1354–1359.
[68] W.A. Smith, T. Burdyny, D.A. Vermaas, H. Geerlings, Pathways to industrial-scale fuel out of thin air from CO_2 electrolysis, Joule 3 (8) (2019) 1822–1834.
[69] C. Delacourt, P.L. Ridgway, J. Newman, Mathematical modeling of CO_2 reduction to CO in aqueous electrolytes: I. Kinetic study on planar silver and gold electrodes, J. Electrochem. Soc. 157 (12) (2010) B1902.
[70] M.R. Singh, K. Papadantonakis, C. Xiang, N.S. Lewis, An electrochemical engineering assessment of the operational conditions and constraints for solar-driven water-splitting systems at near-neutral pH, Energy Environ. Sci. 8 (9) (2015) 2760–2767.
[71] M.R. Thorson, K.I. Siil, P.J. Kenis, Effect of cations on the electrochemical conversion of CO_2 to CO, J. Electrochem. Soc. 160 (1) (2012) F69.
[72] K. Ogura, J.R. Ferrell III, A.V. Cugini, E.S. Smotkin, M.D. Salazar-Villalpando, CO_2 attraction by specifically adsorbed anions and subsequent accelerated electrochemical reduction, Electrochim. Acta 56 (1) (2010) 381–386.
[73] Y. Hori, K. Kikuchi, S. Suzuki, Production of CO and CH_4 in electrochemical reduction of CO_2 at metal electrodes in aqueous hydrogencarbonate solution, Chem. Lett. 14 (11) (1985) 1695–1698.
[74] A.J. Botz, M. Nebel, R.A. Rincón, E. Ventosa, W. Schuhmann, Onset potential determination at gas-evolving catalysts by means of constant-distance mode positioning of nanoelectrodes, Electrochim. Acta 179 (2015) 38–44.
[75] Y. Li, H. Wang, L. Xie, Y. Liang, G. Hong, H. Dai, MoS_2 nanoparticles grown on graphene: an advanced catalyst for the hydrogen evolution reaction, J. Am. Chem. Soc. 133 (19) (2011) 7296–7299.
[76] J. Wu, Y. Huang, W. Ye, Y. Li, CO_2 reduction: from the electrochemical to photochemical approach, Adv. Sci. 4 (11) (2017) 1700194.
[77] C. Zhu, Z. Zhang, L. Zhong, CS. Hsu, X. Xu, Y. Li, S. Zhao, S. Chen, J. Yu, S. Chen, Product-specific active site motifs of Cu for electrochemical CO_2 reduction, Chem. 7 (2) (2021) 406–420.
[78] C.S. Le Duff, M.J. Lawrence, P. Rodriguez, Role of the adsorbed oxygen species in the selective electrochemical reduction of CO_2 to alcohols and carbonyls on copper electrodes, Angew. Chem. 129 (42) (2017) 13099–13104.

[79] Y. Huang, A.D. Handoko, P. Hirunsit, B.S. Yeo, Electrochemical reduction of CO_2 using copper single-crystal surfaces: effects of CO* coverage on the selective formation of ethylene, ACS. Catal. 7 (3) (2017) 1749–1756.

[80] N. Hoshi, M. Kato, Y. Hori, Electrochemical reduction of CO_2 on single crystal electrodes of silver Ag (111), Ag (100) and Ag (110), J. Electroanal. Chem. 440 (1–2) (1997) 283–286.

[81] D. Gao, Y. Zhang, Z. Zhou, F. Cai, X. Zhao, W. Huang, Y. Li, J. Zhu, P. Liu, F. Yang, Enhancing CO_2 electroreduction with the metal–oxide interface, J. Am. Chem. Soc. 139 (16) (2017) 5652–5655.

[82] K. Jiang, Y. Huang, G. Zeng, F.M. Toma, W.A. Goddard III, A.T. Bell, Effects of surface roughness on the electrochemical reduction of CO_2 over Cu, ACS. Energy Lett. 5 (4) (2020) 1206–1214.

[83] S. Wang, B.Y. Guan, X.W.D. Lou, Rationally designed hierarchical N-doped carbon@$NiCo_2O_4$ double-shelled nanoboxes for enhanced visible light CO_2 reduction, Energy Environ. Sci. 11 (2) (2018) 306–310.

[84] Y. Li, X. Li, S. Fan, J. Mu, Z. Yin, H. Ma, S. Wang, Facile tailoring of Co-based spinel hierarchical hollow microspheres for highly efficient catalytic conversion of CO_2, J. Colloid Interface Sci. 552 (2019) 476–484.

[85] X. Li, N. Li, Y. Gao, L. Ge, Design and applications of hollow-structured nanomaterials for photocatalytic H_2 evolution and CO_2 reduction, Chinese J. Catal. 43 (3) (2022) 679–707.

[86] R. Reske, H. Mistry, F. Behafarid, B. Roldan Cuenya, P. Strasser, Particle size effects in the catalytic electroreduction of CO_2 on Cu nanoparticles, J. Am. Chem. Soc. 136 (19) (2014) 6978–6986.

[87] A. Murata, Y. Hori, Product selectivity affected by cationic species in electrochemical reduction of CO_2 and CO at a Cu electrode, Bull. Chem. Soc. Jpn. 64 (1) (1991) 123–127.

[88] L. Han, S. Song, M. Liu, S. Yao, Z. Liang, H. Cheng, Z. Ren, W. Liu, R. Lin, G. Qi, Stable and efficient single-atom Zn catalyst for CO_2 reduction to CH_4, J. Am. Chem. Soc. 142 (29) (2020) 12563–12567.

[89] Y. Hori, K. Kikuchi, A. Murata, S. Suzuki, Production of methane and ethylene in electrochemical reduction of carbon dioxide at copper electrode in aqueous hydrogencarbonate solution, Chem. Lett. 15 (6) (1986) 897–898.

[90] H. Hashiba, S. Yotsuhashi, M. Deguchi, Y. Yamada, Systematic analysis of electrochemical CO_2 reduction with various reaction parameters using combinatorial reactors, ACS Comb. Sci. 18 (4) (2016) 203–208.

[91] S. Kaneco, Nh. Hiei, Y. Xing, H. Katsumata, H. Ohnishi, T. Suzuki, K. Ohta, Electrochemical conversion of carbon dioxide to methane in aqueous $NaHCO_3$ solution at less than 273 K, Electrochim. Acta 48 (1) (2002) 51–55.

[92] S. Kaneco, Nh. Hiei, Y. Xing, H. Katsumata, H. Ohnishi, T. Suzuki, K. Ohta, High-efficiency electrochemical CO_2-to-methane reduction method using aqueous $KHCO_3$ media at less than 273 K, J. Solid. State Electrochem. 7 (3) (2003) 152–156.

[93] M. Azuma, K. Hashimoto, M. Hiramoto, M. Watanabe, T. Sakata, Electrochemical reduction of carbon dioxide on various metal electrodes in low-temperature aqueous $KHCO_3$ media, J. Electrochem. Soc. 137 (6) (1990) 1772.

[94] S.T. Ahn, I. Abu-Baker, G.T.R. Palmore, Electroreduction of CO_2 on polycrystalline copper: effect of temperature on product selectivity, Catal. Today 288 (2017) 24–29.

[95] R. Kas, R. Kortlever, H. Yılmaz, M.T. Koper, G. Mul, Manipulating the hydrocarbon selectivity of copper nanoparticles in CO_2 electroreduction by process conditions, ChemElectroChem. 2 (3) (2015) 354–358.

[96] J. Yu, Q. Wang, D. O'Hare, L. Sun, Preparation of two dimensional layered double hydroxide nanosheets and their applications, Chem. Soc. Rev. 46 (19) (2017) 5950–5974.

[97] X. Liu, R. Ma, Y. Bando, T. Sasaki, Layered cobalt hydroxide nanocones: microwave-assisted synthesis, exfoliation, and structural modification, Angew. Chem. 44 (122) (2010) 8429–8432.

[98] Y. Wang, D. Yan, S. El Hankari, Y. Zou, S. Wang, Recent progress on layered double hydroxides and their derivatives for electrocatalytic water splitting, Adv. Sci. 5 (8) (2018) 1800064.

[99] JM. Oh, CB. Park, JH. Choy, nanotechnology, Intracellular drug delivery of layered double hydroxide nanoparticles, J. Nanosci. Nanotechnol. 11 (2) (2011) 1632–1635.

[100] J.W. Boclair, P.S. Braterman, J. Jiang, S. Lou, F. Yarberry, Layered double hydroxide stability. 2. Formation of Cr (III)-containing layered double hydroxides directly from solution, Chem. Mater. 11 (2) (1999) 303–307.

[101] J.S. Valente, F. Figueras, M. Gravelle, P. Kumbhar, J. Lopez, JP. Besse, Basic properties of the mixed oxides obtained by thermal decomposition of hydrotalcites containing different metallic compositions, J. Catal. 189 (2) (2000) 370–381.

[102] R. Gao, D. Yan, Fast formation of single-unit-cell-thick and defect-rich layered double hydroxide nanosheets with highly enhanced oxygen evolution reaction for water splitting, Nano Res. 11 (2018) 1883–1894.

[103] S. Chen, Z. Kang, X. Hu, X. Zhang, H. Wang, J. Xie, X. Zheng, W. Yan, B. Pan, Y. Xie, Delocalized spin states in 2D atomic layers realizing enhanced electrocatalytic oxygen evolution, Adv. Mater. 29 (30) (2017) 1701687.

[104] J. Zhang, C. Dong, Z. Wang, H. Gao, J. Niu, Z. Peng, Z. Zhang, A new defect-rich CoGa layered double hydroxide as efficient and stable oxygen evolution electrocatalyst, Small. 3 (2) (2019) 1800286.

[105] HF. Wang, C. Tang, BQ. Li, Q. Zhang, A review of anion-regulated multi-anion transition metal compounds for oxygen evolution electrocatalysis, Inorg. Chem. Front. 5 (3) (2018) 521–534.

[106] L. Huang, R. Chen, C. Xie, C. Chen, Y. Wang, Y. Zeng, D. Chen, S. Wang, Rapid cationic defect and anion dual-regulated layered double hydroxides for efficient water oxidation, Nanoscale 10 (28) (2018) 13638–13644.

[107] D. Zhou, Z. Cai, Y. Bi, W. Tian, M. Luo, Q. Zhang, Q. Zhang, Q. Xie, J. Wang, Y. Li, Effects of redox-active interlayer anions on the oxygen evolution reactivity of NiFe-layered double hydroxide nanosheets, Nano Res. 11 (2018) 1358–1368.

[108] Z. Jiang, J. Wu, X. Liu, H. Yu, C. Jiao, J. Shen, Y. Pei, Facile synthesis of MgAl layered double hydroxides by a co-precipitation method for efficient nitrate removal from water: kinetics and mechanisms, New. J. Chem. 45 (32) (2021) 14580–14588.

[109] A. Hussein, K. Burra, G. Bassioni, R. Hammouda, A. Gupta, Production of CO from CO_2 over mixed-metal oxides derived from layered-double-hydroxides, Appl. Energy. 235 (2019) 1183–1191.

[110] Z.P. Xu, G. Stevenson, CQ. Lu, G. Lu, Dispersion and size control of layered double hydroxide nanoparticles in aqueous solutions, J. Phys. Chem. B 110 (34) (2006) 16923–16929.

[111] R. Liu, Y. Wang, D. Liu, Y. Zou, S. Wang, Water-plasma-enabled exfoliation of ultrathin layered double hydroxide nanosheets with multivacancies for water oxidation, Adv. Mater. 29 (30) (2017) 1701546.

[112] Q. Wang, S.V.Y. Tang, E. Lester, D. O'Hare, Synthesis of ultrafine layered double hydroxide (LDHs) nanoplates using a continuous-flow hydrothermal reactor, Nanoscale 5 (1) (2013) 114–117.

[113] W. Wang, Z. Xu, Z. Guo, C. Jiang, W. Chu, Layered double hydroxide and related catalysts for hydrogen production and a biorefinery, Chin. J. Catal. 36 (2) (2015) 139–147.

[114] Z. Zhao, H. Wu, H. He, X. Xu, Y. Jin, A high-performance binary Ni–Co hydroxide-based water oxidation electrode with three-dimensional coaxial nanotube array structure, Adv. Func. Mater. 24 (29) (2014) 4698–4705.

[115] F.L. Theiss, G.A. Ayoko, R. Frost, Synthesis of layered double hydroxides containing Mg^{2+}, Zn^{2+}, Ca^{2+} and Al^{3+} layer cations by co-precipitation methods—A review, Appl. Surf. Sci. 383 (2016) 200–213.

[116] P. Benito, I. Guinea, F. Labajos, J. Rocha, V. Rives, Microwave-hydrothermally aged Zn, Al hydrotalcite-like compounds: influence of the composition and the irradiation conditions, Microporous Mesoporous Mater. 110 (2–3) (2008) 292–302.

[117] V.V. Naik, S. Vasudevan, Effect of alkyl chain arrangement on conformation and dynamics in a surfactant intercalated layered double hydroxide: spectroscopic measurements and MD simulations, J. Phys. Chem. C 115 (16) (2011) 8221–8232.

[118] S. Dou, L. Tao, R. Wang, S. El Hankari, R. Chen, S. Wang, Plasma-assisted synthesis and surface modification of electrode materials for renewable energy, Adv. Mater. 30 (21) (2018) 1705850.

[119] Y. Yu, Z. Bian, F. Song, J. Wang, Q. Zhong, S. Kawi, Influence of calcination temperature on activity and selectivity of Ni–CeO_2 and Ni–$Ce_{0.8}Zr_{0.2}O_2$ catalysts for CO_2 methanation, Top. Catal. 61 (2018) 1514–1527.

[120] G. Fan, F. Li, D.G. Evans, X. Duan, Catalytic applications of layered double hydroxides: recent advances and perspectives, Chem. Soc. Rev. 43 (20) (2014) 7040–7066.

[121] X. Guo, Z. Peng, M. Hu, C. Zuo, A. Traitangwong, V. Meeyoo, C. Li, S. Zhang, Highly active Ni-based catalyst derived from double hydroxides precursor for low temperature CO_2 methanation, Ind. Eng. Chem. Res. 57 (28) (2018) 9102–9111.

[122] F. Zhang, B. Lu, P. Sun, Highly stable Ni-based catalysts derived from LDHs supported on zeolite for CO_2 methanation, Int. J. Hydrogen Energy. 45 (32) (2020) 16183–16192.

[123] D. dos Santos Lima, Y.R. Dias, O. Perez-Lopez, CO_2 methanation over Ni–Al and Co–Al LDH-derived catalysts: the role of basicity, Fuels 4 (11) (2020) 5747–5756.

[124] F. Zhao, L. Fan, K. Xu, D. Hua, G. Zhan, SF. Zhou, Hierarchical sheet-like Cu/Zn/Al nanocatalysts derived from LDH/MOF composites for CO_2 hydrogenation to methanol, J. CO_2 Util. 33 (2019) 222–232.

[125] C. Jeong, YW. Suh, Role of ZrO_2 in Cu/ZnO/ZrO_2 catalysts prepared from the precipitated Cu/Zn/Zr precursors, Catal. Today 265 (2016) 254–263.

[126] Q. Zhu, Q. Zhang, L. Wen, Anti-sintering silica-coating CuZnAlZr catalyst for methanol synthesis from CO hydrogenation, Fuel Process. Technol. 156 (2017) 280–289.

[127] X. Fang, Y. Men, F. Wu, Q. Zhao, R. Singh, P. Xiao, T. Du, P. Webley, Improved methanol yield and selectivity from CO_2 hydrogenation using a novel Cu-ZnO-ZrO_2 catalyst supported on Mg-Al layered double hydroxide (LDH), J. CO2 Util. 29 (2019) 57–64.

[128] S. Xu, E. Carter, Theoretical insights into heterogeneous (photo) electrochemical CO_2 reduction, Chem. Rev. 119 (11) (2018) 6631–6669.

[129] S. Back, M.S. Yeom, Y. Jung, Active sites of Au and Ag nanoparticle catalysts for CO2 electroreduction to CO, ACS. Catal. 5 (9) (2015) 5089–5096.

[130] W. Li, P. Hou, Z. Wang, P. Kang, Synergistic effect of N-doped layered double hydroxide derived NiZnAl oxides in CO_2 electroreduction, Fuels 3 (6) (2019) 1455–1460.

[131] E. Liu, T. Liu, X. Ma, Y. Zhang, The electrocatalytic performance of Ni–AlO (OH) 3@ RGO for the reduction of CO_2 to CO, New. J. Chem. 46 (25) (2022) 12023–12033.

[132] Y. Chen, H. Hong, J. Cai, Z. Li, Highly efficient CO_2 to CO transformation over cu-based catalyst derived from a CuMgAl-layered double hydroxide (LDH), ChemCatChem. 13 (2) (2021) 656–663.

[133] F. Tan, T. Liu, Y.J.J.o.P. Zhang, P.A. Chemistry, Efficient reduction of CO2 to CO by CdAl-LDHs nanostructured electrocatalysts in ionic liquids, (2024), pp. 115518.

[134] H. Furukawa, N. Ko, Y.B. Go, N. Aratani, S.B. Choi, E. Choi, A.Ö. Yazaydin, R. Q. Snurr, M. O'Keeffe, J. Kim, Ultrahigh porosity in metal-organic frameworks, Science (1979) 329 (5990) (2010) 424–428.

[135] O.K. Farha, I. Eryazici, N.C. Jeong, B.G. Hauser, C.E. Wilmer, A.A. Sarjeant, R. Q. Snurr, S.T. Nguyen, A.O.z.r. Yazaydın, J.T. Hupp, Metal–organic framework

materials with ultrahigh surface areas: is the sky the limit? J. Am. Chem. Soc. 134 (36) (2012) 15016–15021.
[136] R. Li, W. Zhang, K. Zhou, Metal–organic-framework-based catalysts for photoreduction of CO2, Adv. Mater. 30 (35) (2018) 1705512.
[137] J.M. Lin, C.T. He, Y. Liu, P.Q. Liao, D.D. Zhou, J.P. Zhang, X.M. Chen, A metal–organic framework with a pore size/shape suitable for strong binding and close packing of methane, Angew. Chem. Int. Ed. 55 (15) (2016) 4674–4678.
[138] B.M. Connolly, M. Aragones-Anglada, J. Gandara-Loe, N.A. Danaf, D.C. Lamb, J. P. Mehta, D. Vulpe, S. Wuttke, J. Silvestre-Albero, P.Z. Moghadam, Tuning porosity in macroscopic monolithic metal-organic frameworks for exceptional natural gas storage, Nat. Commun. 10 (1) (2019) 1–11.
[139] S.M. Rogge, A. Bavykina, J. Hajek, H. Garcia, A.I. Olivos-Suarez, A. Sepúlveda-Escribano, A. Vimont, G. Clet, P. Bazin, F. Kapteijn, Metal–organic and covalent organic frameworks as single-site catalysts, Chem. Soc. Rev. 46 (11) (2017) 3134–3184.
[140] Z. Meng, J. Luo, W. Li, K.A. Mirica, Hierarchical tuning of the performance of electrochemical carbon dioxide reduction using conductive two-dimensional metallophthalocyanine based metal–organic frameworks, J. Am. Chem. Soc. 142 (52) (2020) 21656–21669.
[141] J. Liu, D. Yang, Y. Zhou, G. Zhang, G. Xing, Y. Liu, Y. Ma, O. Terasaki, S. Yang, L. Chen, Tricycloquinazoline-based 2D conductive metal–organic frameworks as promising electrocatalysts for CO_2 reduction, Angew. Chem. Int. Ed. 60 (26) (2021) 14473–14479.
[142] SM. Hwang, S.Y. Choi, M.H. Youn, W. Lee, K.T. Park, K. Gothandapani, A. N. Grace, S.K. Jeong, Investigation on electroreduction of CO_2 to formic acid using $cu_3(btc)_2$ metal–organic framework (cu-mof) and graphene oxide, ACS. Omega 5 (37) (2020) 23919–23930.
[143] P. Lamagni, M. Miola, J. Catalano, M.S. Hvid, M.A.H. Mamakhel, M. Christensen, M.R. Madsen, H.S. Jeppesen, X.M. Hu, K. Daasbjerg, Restructuring metal–organic frameworks to nanoscale bismuth electrocatalysts for highly active and selective CO_2 reduction to formate, Adv. Funct. Mater. 30 (16) (2020) 1910408.
[144] F. Yang, A. Chen, P.L. Deng, Y. Zhou, Z. Shahid, H. Liu, B.Y. Xia, Highly efficient electroconversion of carbon dioxide into hydrocarbons by cathodized copper–organic frameworks, Chem. Sci. 10 (34) (2019) 7975–7981.
[145] F. Guo, S. Yang, Y. Liu, P. Wang, J. Huang, WY. Sun, Size engineering of metal–organic framework MIL-101 (Cr)–Ag hybrids for photocatalytic CO_2 reduction, ACS. Catal. 9 (9) (2019) 8464–8470.
[146] SQ. Wang, XY. Zhang, XY. Dao, XM. Cheng, WY. Sun, Cu_2O@ Cu@ UiO-66-NH_2 ternary nanocubes for photocatalytic CO_2 reduction, ACS Appl. Nano Mater. 3 (10) (2020) 10437–10445.
[147] XY. Dao, XF. Xie, JH. Guo, XY. Zhang, YS. Kang, WY. Sun, Boosting photocatalytic CO_2 reduction efficiency by heterostructures of NH_2-MIL-101 (Fe)/g-C_3N_4, ACS Appl. Energy Mater. 3 (4) (2020) 3946–3954.
[148] L. Zhao, Z. Zhao, Y. Li, X. Chu, Z. Li, Y. Qu, L. Bai, L. Jing, The synthesis of interface-modulated ultrathin Ni (ii) MOF/gC_3N_4 heterojunctions as efficient photocatalysts for CO_2 reduction, Nanoscale 12 (18) (2020) 10010–10018.
[149] L. Chen, Y. Wang, F. Yu, X. Shen, C. Duan, A simple strategy for engineering heterostructures of Au nanoparticle-loaded metal–organic framework nanosheets to achieve plasmon-enhanced photocatalytic CO_2 conversion under visible light, J. Mater. Chem. A 7 (18) (2019) 11355–11361.
[150] X. Deng, J. Albero, L. Xu, H. Garcia, Z. Li, Construction of a stable Ru–Re hybrid system based on multifunctional MOF-253 for efficient photocatalytic CO_2 reduction, Inorg. Chem. 57 (14) (2018) 8276–8286.
[151] Y. Liu, JH. Guo, XY. Dao, XD. Zhang, Y. Zhao, WY. Sun, Coordination polymers with a pyridyl–salen ligand for photocatalytic carbon dioxide reduction, Chem. Commun. 56 (29) (2020) 4110–4113.
[152] Y. Wang, NY. Huang, JQ. Shen, PQ. Liao, XM. Chen, JP. Zhang, Hydroxide ligands cooperate with catalytic centers in metal–organic frameworks for efficient photocatalytic CO_2 reduction, J. Am. Chem. Soc. 140 (1) (2018) 38–41.
[153] L. Shen, W. Wu, R. Liang, R. Lin, L. Wu, Highly dispersed palladium nanoparticles anchored on UiO-66 (NH 2) metal-organic framework as a reusable and dual functional visible-light-driven photocatalyst, Nanoscale 5 (19) (2013) 9374–9382.
[154] Y. Zhang, X. Bo, A. Nsabimana, C. Han, M. Li, L. Guo, Electrocatalytically active cobalt-based metal–organic framework with incorporated macroporous carbon composite for electrochemical applications, J. Mater. Chem. A 3 (2) (2015) 732–738.
[155] W.J. Phang, W.R. Lee, K. Yoo, D.W. Ryu, B. Kim, C.S. Hong, pH-dependent proton conducting behavior in a metal–organic framework material, Angew. Chem. Int. Ed. 126 (32) (2014) 8523–8527.
[156] N. Campagnol, E.R. Souza, D.E. De Vos, K. Binnemans, J. Fransaer, Luminescent terbium-containing metal–organic framework films: new approaches for the electrochemical synthesis and application as detectors for explosives, Chem. Commun. 50 (83) (2014) 12545–12547.
[157] M.Y. Masoomi, A. Morsali, P.C. Junk, Rapid mechanochemical synthesis of two new Cd (II)-based metal–organic frameworks with high removal efficiency of Congo red, CrystEngComm. 17 (3) (2015) 686–692.
[158] M. Song, X. Song, X. Liu, W. Zhou, P. Huo, Enhancing photocatalytic CO_2 reduction activity of $ZnIn_2S_4$/MOF-808 microsphere with S-scheme heterojunction by in situ synthesis method, Chinese J. Catal. 51 (2023) 180–192.
[159] F.X.L. i Xamena, J. Gascon, Metal organic frameworks as heterogeneous catalysts, Royal Society Chem. (2013).
[160] C.P. Raptopoulou, Metal-organic frameworks: synthetic methods and potential applications, Materials. (Basel) 14 (2) (2021) 310.
[161] E. Mouafo-Tchinda, J.C. Kemmegne-Mbouguen, C.P. Nanseu-Njiki, H.W. Langmi, C. Kowenje, N.M. Musyoka, R. Mokaya, Solvothermal synthesis of organoclay/Cu-MOF composite and its application in film modified GCE for simultaneous electrochemical detection of deoxyepinephrine, acetaminophen and tyrosine, RSC. Adv. 13 (30) (2023) 20816–20829.
[162] G.A. Tompsett, W.C. Conner, K.S. Yngvesson, Microwave synthesis of nanoporous materials, Chemphyschem. 7 (2) (2006) 296–319.
[163] T. Friščić, Metal-organic frameworks: mechanochemical synthesis strategies, Encyclopedia Inorganic Bioinorganic Chem. (2011) 1–19.
[164] JX. Wu, WW. Yuan, M. Xu, ZY. Gu, Ultrathin 2D nickel zeolitic imidazolate framework nanosheets for electrocatalytic reduction of CO_2, Chem. Commun. 55 (77) (2019) 11634–11637.
[165] X.D. Zhang, S.Z. Hou, J.X. Wu, Z.Y. Gu, Two-dimensional metal–organic framework nanosheets with cobalt-porphyrins for high-performance co2 electroreduction, Chem. - Eur. J. 26 (7) (2020) 1604–1611.
[166] Y. Wang, P. Hou, Z. Wang, P. Kang, Zinc imidazolate metal–organic frameworks (ZIF-8) for electrochemical reduction of CO_2 to CO, Chemphyschem. 18 (22) (2017) 3142–3147.
[167] X. Jiang, H. Li, J. Xiao, D. Gao, R. Si, F. Yang, Y. Li, G. Wang, X. Bao, Carbon dioxide electroreduction over imidazolate ligands coordinated with Zn (II) center in ZIFs, Nano Energy 52 (2018) 345–350.
[168] N. Kornienko, Y. Zhao, C.S. Kley, C. Zhu, D. Kim, S. Lin, C.J. Chang, O.M. Yaghi, P. Yang, Metal–organic frameworks for electrocatalytic reduction of carbon dioxide, J. Am. Chem. Soc. 137 (44) (2015) 14129–14135.
[169] Q. Huang, Q. Li, J. Liu, R. Wang, YQ. Lan, Disclosing CO2 activation mechanism by hydroxyl-induced crystalline structure transformation in electrocatalytic process, Matter. 1 (6) (2019) 1656–1668.
[170] BX. Dong, SL. Qian, FY. Bu, YC. Wu, LG. Feng, YL. Teng, WL. Liu, ZW. Li, Electrochemical reduction of CO_2 to CO by a heterogeneous catalyst of Fe–porphyrin-based metal–organic framework, ACS Appl. Energy Mater. 1 (9) (2018) 4662–4669.
[171] I. Hod, M.D. Sampson, P. Deria, C.P. Kubiak, O.K. Farha, J.T. Hupp, Fe-porphyrin-based metal–organic framework films as high-surface concentration, heterogeneous catalysts for electrochemical reduction of CO_2, ACS. Catal. 5 (11) (2015) 6302–6309.
[172] CW. Kung, C.O. Audu, A.W. Peters, H. Noh, O.K. Farha, J.T. Hupp, Copper nanoparticles installed in metal–organic framework thin films are electrocatalytically competent for CO_2 reduction, ACS. Energy Lett. 2 (10) (2017) 2394–2401.
[173] P. De Luna, W. Liang, A. Mallick, O. Shekhah, F.P. García de Arquer, A.H. Proppe, P. Todorović, S.O. Kelley, E.H. Sargent, M. Eddaoudi, Metal–organic framework thin films on high-curvature nanostructures toward tandem electrocatalysis, ACS Appl. Mater. Interfaces 10 (37) (2018) 31225–31232.
[174] Y.T. Guntern, J.R. Pankhurst, J. Vávra, M. Mensi, V. Mantella, P. schouwink, r. buonsanti, nanocrystal/metal–organic framework hybrids as electrocatalytic platforms for CO_2 conversion, Angew. Chem. Int. Ed. 58 (36) (2019) 12632–12639.
[175] R. Hinogami, S. Yotsuhashi, M. Deguchi, Y. Zenitani, H. Hashiba, Y. Yamada, Electrochemical reduction of carbon dioxide using a copper rubeanate metal organic framework, ECS Electrochem. Lett 1 (4) (2012) H17–H19.
[176] R.S. Kumar, S.S. Kumar, M.A. Kulandainathan, Highly selective electrochemical reduction of carbon dioxide using Cu based metal organic framework as an electrocatalyst, Electrochem. Commun. 25 (2012) 70–73.
[177] X. Kang, B. Wang, K. Hu, K. Lyu, X. Han, B.F. Spencer, M.D. Frogley, F. Tuna, E. J. McInnes, R.A. Dryfe, Quantitative electro-reduction of CO_2 to liquid fuel over electro-synthesized metal–organic frameworks, J. Am. Chem. Soc. 142 (41) (2020) 17384–17392.
[178] J. Albo, D. Vallejo, G. Beobide, O. Castillo, P. Castaño, A. Irabien, Copper-based metal–Organic porous materials for CO_2 electrocatalytic reduction to alcohols, ChemSusChem. 10 (6) (2017) 1100–1109.
[179] J. Albo, M. Perfecto-Irigaray, G. Beobide, A. Irabien, Cu/Bi metal-organic framework-based systems for an enhanced electrochemical transformation of CO_2 to alcohols, J J. CO_2 Util. 33 (2019) 157–165.
[180] M. Perfecto-Irigaray, J. Albo, G. Beobide, O. Castillo, A. Irabien, S. Pérez-Yáñez, Synthesis of heterometallic metal–organic frameworks and their performance as electrocatalyst for CO_2 reduction, RSC. Adv. 8 (38) (2018) 21092–21099.
[181] S. Chen, W.H. Li, W. Jiang, J. Yang, J. Zhu, L. Wang, H. Ou, Z. Zhuang, M. Chen, X. Sun, MOF encapsulating N-heterocyclic carbene-ligated copper single-atom site catalyst towards efficient methane electrosynthesis, Angew. Chem. Int. Ed. 61 (4) (2022) e202114450.
[182] Y. Zhao, H. Zhou, X. Zhu, Y. Qu, C. Xiong, Z. Xue, Q. Zhang, X. Liu, F. Zhou, X. Mou, Simultaneous oxidative and reductive reactions in one system by atomic design, Nat. Catal. 4 (2) (2021) 134–143.
[183] X. Zhang, D. Xue, S. Jiang, H. Xia, Y. Yang, W. Yan, J. Hu, J. Zhang, Rational confinement engineering of MOF-derived carbon-based electrocatalysts toward CO2 reduction and O_2 reduction reactions, InfoMat 4 (3) (2022) e12257.
[184] K. Zhao, Y. Liu, X. Quan, S. Chen, H. Yu, CO_2 electroreduction at low overpotential on oxide-derived Cu/carbons fabricated from metal organic framework, ACS Appl. Mater. Interfaces 9 (6) (2017) 5302–5311.
[185] W. Zhang, Y. Hu, L. Ma, G. Zhu, Y. Wang, X. Xue, R. Chen, S. Yang, Z. Jin, Progress and perspective of electrocatalytic CO_2 reduction for renewable carbonaceous fuels and chemicals, Adv. Sci. 5 (1) (2018) 1700275.
[186] P. Shao, L. Yi, S. Chen, T. Zhou, J. Zhang, Metal-organic frameworks for electrochemical reduction of carbon dioxide: the role of metal centers, J. Energy Chem. (2019).
[187] Y. Shang, X. Xu, Z. Wang, B. Jin, R. Wang, Z. Ren, B. Gao, Q. Yue, rGO/CNTs supported pyrolysis derivatives of $[Mo_3S_{13}]_2$–clusters as promising

electrocatalysts for enhancing hydrogen evolution performances, ACS Sustain. Chem. Eng. 6 (5) (2018) 6920–6931.
[188] JX. Wu, SZ. Hou, XD. Zhang, M. Xu, HF. Yang, PS. Cao, ZY. Gu, Cathodized copper porphyrin metal–organic framework nanosheets for selective formate and acetate production from CO_2 electroreduction, Chem. Sci. 10 (7) (2019) 2199–2205.
[189] X. Tan, C. Yu, C. Zhao, H. Huang, X. Yao, X. Han, W. Guo, S. Cui, H. Huang, J. Qiu, Restructuring of Cu_2O to Cu_2O@ Cu-metal–organic frameworks for selective electrochemical reduction of CO_2, ACS Appl. Mater. Interfaces 11 (10) (2019) 9904–9910.
[190] Y. Guo, H. Yang, X. Zhou, K. Liu, C. Zhang, Z. Zhou, C. Wang, W. Lin, Electrocatalytic reduction of CO_2 to CO with 100% faradaic efficiency by using pyrolyzed zeolitic imidazolate frameworks supported on carbon nanotube networks, J. Mater. Chem. A 5 (47) (2017) 24867–24873.
[191] X. Jiang, H. Wu, S. Chang, R. Si, S. Miao, W. Huang, Y. Li, G. Wang, X. Bao, Boosting CO_2 electroreduction over layered zeolitic imidazolate frameworks decorated with Ag_2 O nanoparticles, J. Mater. Chem. A 5 (36) (2017) 19371–19377.
[192] X. Wang, Z. Chen, X. Zhao, T. Yao, W. Chen, R. You, C. Zhao, G. Wu, J. Wang, W. Huang, Regulation of coordination number over single Co sites: triggering the efficient electroreduction of CO_2, Angew. Chem. Int. Ed. 57 (7) (2018) 1944–1948.
[193] Y. Zheng, P. Cheng, J. Xu, J. Han, D. Wang, C. Hao, H.R. Alanagh, C. Long, X. Shi, Z. Tang, MOF-derived nitrogen-doped nanoporous carbon for electroreduction of CO_2 to CO: the calcining temperature effect and the mechanism, Nanoscale 11 (11) (2019) 4911–4917.